

AEROTHERM CORPORATION

RESEARCH & DEVELOPMENT IN AEROTHERMOCHEMISTRY



FINAL REPORT

FURTHER STUDIES OF THE COUPLED
CHEMICALLY REACTING BOUNDARY
LAYER AND CHARRING ABLATOR

PART I SUMMARY REPORT

by
E.P. Bartlett, W.E. Nicolet
L.W. Anderson, R.M. Kendall

FACILITY FORM 602

N 69-17790

(ACCESSION NUMBER)

(THRU)

(PAGES)

(CODE)

NASA-CR 92471

(NASA CR OR TMX OR AD NUMBER)

(CATEGORY)

NASA CR 92471

Aerotherm Report No. 68-38, Part I
Copy No. ____

FINAL REPORT

FURTHER STUDIES OF THE COUPLED CHEMICALLY
REACTING BOUNDARY LAYER AND CHARRING ABLATOR

PART I
SUMMARY REPORT

by

Eugene P. Bartlett, William E. Nicolet
Larry W. Anderson, Robert M. Kendall

Prepared for

NATIONAL AERONAUTICS AND SPACE ADMINISTRATION

October 15, 1968

CONTRACT NAS9-6719

Technical Management
NASA Manned Spacecraft Center
Houston, Texas
Structures and Mechanics Division
D. M. Curry
G. Strouhal

ABSTRACT

This report summarizes a substantial analytical effort which is reported in more detail in Parts II through IV of this series of reports. The primary result of this effort has been the development of a number of computer codes applicable to charring ablation materials and chemically reacting laminar boundary layers and the initiation of a turbulent boundary layer development. These programs can be operated independently or used in conjunction with each other to obtain various degrees of coupling. The basic programs predict the transient in-depth response of charring ablation materials, the chemical state of open or closed systems, nongrey radiation flux distributions, and nonsimilar laminar multicomponent chemically-reacting (equilibrium) boundary layers. The radiation code has been coupled into the boundary layer code to predict radiation-coupled nonsimilar laminar flows; the charring ablation program is used in conjunction with the chemistry program (although mechanically decoupled) to provide an economical means for predicting coupled transient response of charring materials with the boundary layer represented by transfer coefficients; and the laminar boundary layer and charring ablations programs are used to predict transient response of charring materials fully coupled to laminar nonsimilar boundary layers. The charring ablation model considers one-dimensional heat and mass transfer along thermal streamtubes of arbitrary cross-sectional area; the radiation model considers continuum transitions, molecular bands, and atomic lines of the C-H-O-N system in obtaining radiation properties and fluxes; and the chemistry and boundary layer procedures apply to general chemical systems and consider rate-controlled surface reactions. The turbulent boundary layer code currently considers nonsimilar constant-property flows with mass injection.

FOREWORD

The present report is one of a series of four reports, published simultaneously, which describe extension and application of analyses and computational procedures for predicting the in-depth response of charring ablation materials and non-similar chemically reacting boundary layers which were generated under a previous contract (NAS9-4599). In particular, the present reports describe the extension of a laminar multicomponent chemically-reacting (equilibrium) boundary-layer program to include nongrey radiation coupling, the extension of this computational procedure to turbulent flow (at this point for incompressible flows only), the further checkout of a code which couples the laminar boundary layer procedure to a transient charring ablation code, and the application of these and other computational procedures to the Apollo heat shield material and typical Apollo missions. Part I serves as a summary report and describes the present status of and solutions obtained with the various computational procedures. In Part II a thermochemical ablation program based on a transfer-coefficient approach is utilized to investigate ablation mechanisms for the Apollo heat shield material. The radiation transport model which is utilized is described in Part III, whereas the turbulent boundary layer code is discussed in Part IV.

The titles in the series are:

- Part I: Summary Report: Further Studies of the Coupled Chemically Reacting Boundary Layer and Charring Ablator, by E.P. Bartlett, W.E. Nicolet, L.W. Anderson, and R.M. Kendall.
- Part II: An Evaluation of Surface Recession Models for the Apollo Heat Shield Material, by E.P. Bartlett, and L. W. Anderson.
- Part III: A Nongrey Radiation Transport Model Suitable for Use in Ablation-Product Contaminated Boundary Layers, by W. E. Nicolet
- Part IV: Nonsimilar Solution of an Incompressible Turbulent Boundary Layer by an Integral Matrix Method, by L. W. Anderson and R. M. Kendall.

This effort was conducted for the Structures and Mechanics Division of the Manned Spacecraft Center, National Aeronautics and Space Administration under Contract NAS9-6719 with Mr. Donald M. Curry as the NASA Technical Monitor. Development of the turbulent boundary layer code was sponsored jointly by NASA/MSC and by the Air Force Weapons Laboratory, Kirtland Air Force Base, with Lt. Ronald H. Aungier as Project Engineer. Extension of the turbulent boundary layer analysis to compressible flows is continuing under AFWL sponsorship. Mr. Eugene P. Bartlett of Aerotherm Corporation was Program Manager and Principal Investigator for the efforts reported here.

TABLE OF CONTENTS

<u>Section</u>	<u>Title</u>	<u>Page</u>
	ABSTRACT	ii
	FOREWORD	iii
	LIST OF TABLES	v
	LIST OF FIGURES	v
	LIST OF SYMBOLS	viii
1	INTRODUCTION	1
2	SUMMARY OF COMPUTER CODES DEVELOPED UNDER PREVIOUS EFFORT	2
	2.1 Boundary Layer Integral Matrix Procedure (BLIMP)	2
	2.2 Charring Material Ablation (CMA) Program	6
	2.3 Aerotherm Chemical Equilibrium (ACE) Program	9
	2.4 CMA/ACE Coupling Procedure	12
	2.5 Coupled Ablator/Boundary Layer/Environment (CABLE) Program	14
3	ANALYSIS AND COMPUTATIONAL PROCEDURE FOR SOLUTION OF INCOMPRESSIBLE TURBULENT BOUNDARY LAYERS (SAINT PROGRAM)	21
	3.1 General	21
	3.2 Basic Equations and Turbulent Model	21
	3.2.1 General Equations of Motion	21
	3.2.2 Law of the Wall Region	22
	3.2.3 Wake Region	25
	3.3 Solution Procedure	27
	3.4 The SAINT Boundary Layer Program	28
	3.5 Concluding Remarks	29
4	ANALYSIS AND COMPUTATIONAL PROCEDURE FOR THE EVALUATION OF NONGREY RADIANT HEAT FLUX (RAD PROGRAM)	30
	4.1 General	30
	4.2 Absorption Coefficients of the Boundary Layer Species	30
	4.2.1 Atomic and Ionic Continuum Transitions	30
	4.2.2 Atomic Line Transitions	31
	4.2.3 Molecular Band Transitions	33
	4.2.4 Other Transitions	33
	4.2.5 Numerical Evaluation of the Radiation Properties Model	34
	4.3 Transport Model and Numerical Solution Procedure	34
	4.3.1 Formulation	34
	4.3.2 Numerical Evaluation of Flux Integrals	36
	4.4 The Radiation Transport Program (RAD)	37
	4.4.1 Program Objectives	37
	4.4.2 Program Input Requirements	38
	4.4.3 Program Capabilities	38
	4.4.4 Program Storage Requirements and Computational Time	39
	4.4.5 Program Utilization	39
	4.5 Concluding Remarks	39
5	ANALYSIS AND COMPUTATIONAL PROCEDURE FOR RADIATION COUPLED BOUNDARY LAYERS (RABLE PROGRAM)	40
	5.1 Formulation	40
	5.2 Solution Procedure	41
	5.3 The RABLE Program	41

TABLE OF CONTENTS (concluded)

<u>Section</u>	<u>Title</u>	<u>Page</u>
6	APPLICATION OF CODES TO APOLLO HEAT SHIELD PROBLEMS	43
	6.1 Introduction	43
	6.2 Driver Temperature Calculations Using CMA Option 2	43
	6.3 Normalized Ablation Tables Generated by ACE Program	44
	6.4 Steady-State Ablation Predictions Using BLIMP	46
	6.4.1 Solutions for a Recent Superorbital Apollo Flight	46
	6.4.2 Solutions for a 50,000 Feet-Per-Second Trajectory	47
	6.5 Uncoupled Calculation of Radiative Flux Distribution Using the RAD Program	52
	6.6 A Calculation of the Radiation Coupled Boundary Layer Using the RABLE Program	56
	6.7 Coupled Transient Solutions Using CMA/ACE Approach	57
	6.8 Coupled Transient Solution Using CABLE Program	58
7	SUMMARY AND RECOMMENDATIONS	62
	REFERENCES	64
	APPENDIX A - AN ILLUSTRATION OF THE CABLE COUPLING PROCEDURE FOR A TYPICAL APOLLO SUPERORBITAL REENTRY TRAJECTORY	

LIST OF TABLES

<u>Table</u>	<u>Title</u>	<u>Page</u>
I	Coupled Ablator/Boundary Layer/Environment (CABLE) Computer Program	15
II	NASA 50,000 fps Trajectory	48
III	CABLE Results for Temperature Distributions Through the Charring Ablator and Boundary Layer, Pyrolysis Gas Rates, and Char Recession Rates: Apollo Stagnation Point During Typical Superorbital Reentry	60

LIST OF FIGURES

<u>Figure</u>	<u>Title</u>	<u>Page</u>
1.	Correlation of In-Depth Temperature Response of Apollo Flight Data Using 0.3-Inch Thermocouple as a Driver	44
2.	Comparison with Ground Test Data of Noncoking Fissure Surface Thermochemistry Model Including $B_c \sqrt{P}$ Correlation for Mechanical Removal of Silica	45
3.	Comparison of Surface Thermochemistry Maps for Non-fissure Model with Rate Law for Mechanical Removal of Silica as Generated by BLIMP and ACE Programs ($H_T = 25,000$ Btu/lb, $P_{T_2} = 0.028$ atm)	46

LIST OF FIGURES (continued)

<u>Figure</u>	<u>Title</u>	<u>Page</u>
4.	Boundary Layer Solutions Along Apollo Windward Ray for Fissure and Nonfissure Models Considering Steady-State Surface Energy Balances for Typical Superorbital Trajectory (Time = 30,030 sec)	
	(a) Surface Recession Rate	47
	(b) Surface Temperature	47
5.	Convective and Radiative Heating Rates to Stagnation Point of Apollo Vehicle During Typical 50,000 fps Reentry	49
6.	Temperature Distributions Across Apollo Stagnation Point Boundary Layer During Typical 50,000 fps Reentry	49
7.	Mole Fractions Across Apollo Stagnation Point Boundary Layer During Typical 50,000 fps Reentry	50
8.	Surface Temperature History for Apollo Stagnation Point During Typical 50,000 fps Reentry	51
9.	Surface Recession Rate History for Apollo Stagnation Point During Typical 50,000 fps Reentry	51
10.	Surface Recession History for Apollo Stagnation Point During Typical 50,000 fps Reentry	52
11.	Correlation of Surface Recession Rate Versus Radiative Heat Flux for Apollo Stagnation Point During Typical 50,000 fps Reentry	52
12.	Effect of the Radiative Coupling on the Temperature Distribution for Typical Apollo Superorbital Trajectory (Time = 30,045 sec)	53
13.	Effect of Coupling on the Spatial Distribution of the Radiating Species for Typical Apollo Superorbital Trajectory (Time = 30,045 sec)	53
14.	Spatial Distributions of the Radiative Fluxes in the Positive and Negative Directions for Typical Apollo Superorbital Trajectory (Time = 30,045 sec)	54
15.	Components of the Radiative Flux Directed Toward the Wall for Typical Apollo Superorbital Trajectory (Time = 30,045 sec)	54
16.	Spectral Distribution of the Continuum Flux Directed Toward the Wall for Typical Apollo Superorbital Trajectory (Time = 30,045 sec)	55
17.	Effect of Radiative Coupling on the Net Radiative Flux Distribution for Typical Apollo Superorbital Trajectory (Time = 30,045 sec)	55

LIST OF FIGURES (concluded)

<u>Figure</u>	<u>Title</u>	<u>Page</u>
18.	Temperature Histories for Typical Superorbital Trajectory with Fissure and Post-Peak Fissure Models	
	(a) Surface Temperature	57
	(b) 0.3 Inch from Initial Surface	57
	(c) 0.9 Inch from Initial Surface	58
19.	Surface Recession Rate Histories for Typical Superorbital Trajectory with Fissure and Post-Peak Fissure Models	58
20.	Elemental Mass Fractions Across Apollo Stagnation Point Boundary Layer During Typical Superorbital Reentry (Time = 30,020 sec)	59

LIST OF SYMBOLS

b	line shape function
B	Planck function
B'_c	$\dot{m}_c / \rho_e u_e C_M$
B'_g	$\dot{m}_g / \rho_e u_e C_M$
c	speed of light
E	black body emissive power
e	charge on an electron
\mathcal{E}_n	exponential integral of order n
F^\pm	one-sided radiative flux
f	stream function; oscillator strength of a line
h	Planck's constant
H_T	total enthalpy
k	Boltzmann's constant
K	Prandtl mixing length constant
K_C	Clauser parameter
l	mixing length
m	mass of an electron
\dot{m}_c	char mass ablation rate
\dot{m}_g	pyrolysis gas mass flow rate
N	number density
P	pressure
q	net flux
Re_δ	Reynolds number based on δ
r_o	local radius for axisymmetric body
s	streamwise distance
\dot{s}	surface linear recession rate

LIST OF SYMBOLS (continued)

T	temperature
u	velocity in s direction
v	velocity in y direction
y	normal spatial coordinate
y_a^+	proportionality constant in mixing length relation

GREEK SYMBOLS

α_H	normalizing parameter used in definition of η
β	streamwise pressure-gradient parameter
δ	reference thickness defined by Equation (19)
δ^*	boundary layer displacement thickness
ϵ	emissivity; eddy viscosity
η	transformed coordinate for boundary-layer normal direction (defined differently for laminar and turbulent boundary layers)
θ	time
μ	shear viscosity; absorption coefficient
μ'	absorption coefficient corrected for induced emission
ν	kinematic viscosity; photon frequency
ξ	transformed coordinate for boundary-layer streamwise direction (defined differently for laminar and turbulent boundary layers)
ρ	density
$\rho_e^{u C_M}$	mass transfer coefficient
τ	shear; optical depth
ϕ	intermittency factor

LIST OF SYMBOLS (concluded)

SUBSCRIPTS

e	boundary layer edge
i	species i
j	absorbing level j
k	element k; line ν
w	wall
ν	spectral quantity

SUPERSCRIPTS

C	continuum quantity
L	line property
κ	unity for axisymmetric and zero for planar flows
*	normalized by $\rho_e u_e \mu_e r_o^\kappa / (2\xi)^{1/2}$; condensed species
'	(prime) fluctuating quantity; derivative with respect to η
—	averaged quantity

FURTHER STUDIES OF THE COUPLED CHEMICALLY REACTING BOUNDARY LAYER AND CHARRING ABLATOR

SECTION 1

INTRODUCTION

In a previous effort, reported in Reference 1, analyses and computational procedures were developed for representing laminar nonsimilar chemically-reacting boundary layer for general chemical systems, for representing one-dimensional charring ablation response, and for coupling these procedures. In the ensuing eighteen months these procedures have been exercised extensively until they now might be considered fully operational. In addition, the boundary layer procedure has been extended to include nongrey radiation absorption and emission and a turbulent boundary layer development has been initiated.

The codes developed under the previous effort are summarized in Section 2. These consist of the laminar boundary layer procedure, the charring ablation procedure, a chemical state routine which among other options evaluates surface ablation phenomena in terms of convective transfer coefficients, and procedures for coupling the charring ablation routine with the transfer coefficient approach and with the boundary layer procedure. A turbulent constant properties nonsimilar solution procedure is summarized in Section 3 and discussed in detail in Part IV of the present series of reports. An analysis and computational procedure for evaluating nongrey radiant heat flux is summarized in Section 4 and discussed in detail in Part III of the present series of reports. A procedure which couples this radiation routine into the laminar boundary layer program is described in Section 5. Solutions generated with these codes for various Apollo superorbital reentry problems are presented in Section 6, whereas a detailed evaluation of the Apollo heat shield material response is presented in Part II of the present series of reports. Summary and recommendations are presented in Section 7.

SECTION 2

SUMMARY OF COMPUTER CODES DEVELOPED UNDER PREVIOUS EFFORT

A number of mutually compatible computer codes for representing coupled or uncoupled chemically reacting boundary layers and charring ablators were developed under a previous effort. The resulting computer codes are summarized in Reference 1 and described in detail in References 2 through 5. These codes are identified as follows:

- a. Charring Material Ablation (CMA) program
- b. Boundary Layer Integral Matrix Procedure (BLIMP)
- c. Aerotherm Chemical Equilibrium (ACE) program
- d. Coupled Ablator/Boundary Layer/Environment (CABLE) program

The CMA program can be operated independently for obtaining the in-depth response of charring (or noncharring) materials for assigned ablation rates and surface temperatures. The ACE program can be operated independently to determine the equilibrium chemical state for a variety of open and closed systems of arbitrary elemental composition and, in one option, provides surface chemistry and mass-balance tabular data to the CMA program for transient charring ablation calculations. (In this surface state option the name ACE is somewhat misleading because the capability exists to consider rate-controlled surface reactions.) The BLIMP program can be operated independently to provide nonsimilar laminar multicomponent boundary layer solutions for a variety of uncoupled, partially coupled, or coupled steady-state ablation surface boundary conditions. Finally, the CABLE program calls the CMA and BLIMP programs as subroutines to provide fully coupled transient charring ablation solutions. The present status of these routines is summarized in the following subsections.

2.1 BOUNDARY LAYER INTEGRAL MATRIX PROCEDURE (BLIMP)

The BLIMP program solves the nonsimilar two-dimensional or axisymmetric laminar boundary layer by a novel procedure which is capable in a practical limit of yielding "exact" solutions for the equations considered. The equations which are solved, the solution procedure which is utilized, and the characteristics of the program are described in detail in Reference 3 and are summarized in Reference 1. A comprehensive up-to-date user's manual is available as Reference 6. The program is virtually unchanged since the writing of References 1 and 3 with regard to the physical and chemical models which are considered and the basic solution procedure which is utilized. However, many detailed improvements have been made, particularly in the convergence procedure,

which have elevated the program to an operational status. Therefore, the present discussion will be limited to a brief discussion of the current status of the program; the reader is referred to References 1 and 3 for further details.

The BLIMP program applies to general chemical systems, considering equilibrium with the exception that selected species or component mixtures can be considered to be frozen, and rate-controlled surface reactions or surface-catalyzed homogeneous reactions can be taken into account. Multicomponent diffusion and thermal diffusion are treated through the use of convenient correlation equations for binary diffusion coefficients and for multicomponent thermal diffusion coefficients, respectively, described in Reference 4.

The surface boundary condition admits discontinuous injection of chemically-reacting component mixtures such as one might define for a char and pyrolysis gas. These injection rates can be assigned together with surface temperature; surface equilibrium or rate-controlled surface reactions can be specified for assigned injection rates or assigned surface temperature; or surface equilibrium with a steady-state surface energy balance can be considered. The BLIMP code also serves as a subroutine to the CABLE program in which case the CMA program provides to BLIMP, in effect, a transient surface energy balance (this is discussed in Section 2.5).

The BLIMP program calculates its own boundary-layer edge condition by performing an isentropic expansion given stagnation conditions and pressure distribution around the body. An incident radiation flux can be taken into account when a surface energy balance is considered. This incident flux is considered to enter into the surface energy balance without being attenuated in the boundary layer. (A procedure for obtaining radiation-coupled boundary layer solutions, termed the RABLE code, is described in Section 5.)

The boundary-layer equations are transformed into modified Levy-Lees coordinates, η and ξ , the modification being that the normal boundary layer coordinate η is stretched by a variable $\alpha_H(\xi)$ which is determined during the course of the calculation by a constraint such that the nodal system grows (or shrinks) with the boundary layer thickness.

The numerical solution procedure which is employed, termed an integral-matrix method, was developed specifically for the present requirements. In particular, it was desired to minimize the number of entries into the conservation equations because of the relatively large times associated with the

determination of the state for a general chemical environment and to take large steps in the streamwise direction since the boundary layer procedure was to be coupled to an in-depth conduction solution.

For a given accuracy, the number of entries into the conservation equations necessary for solution in the surface normal direction is controlled primarily by the nature of the functions which relate the dependent variables (and their derivatives) to the independent variable. Thus the continuous functions typically used in integral relations approaches require fewer entries than the discontinuous functions implied by most finite difference approximations. In order to permit relatively flexible profiles, sets of connected quadratics* were selected to relate total enthalpy, velocity ratio, and elemental mass fractions to their derivatives with respect to η through the use of Taylor series expansions. The derivatives of these quadratics are continuous at the connecting points resulting in smooth but flexible profiles.

Following the general integral relations phraseology, weighting functions must be selected.** In the present development, this selection was based primarily on the complexity of the resultant algebra. Calculations performed (Reference 3) using a differential approach and using step weighting functions similar to those used by Pallone (Reference 8), indicated, when other aspects of the procedure were unchanged, no apparent superiority with regard to accuracy or stability. Because all of the complexities introduced by the generalization of the thermodynamic and transport properties of the system occur within divergence terms, square-wave weighting functions produce markedly simpler algebra and, consequently, were adopted for the present procedure.

In order to achieve relatively large spacing in the streamwise direction, an iterative procedure is used to assure accuracy and stability. The specific treatment adopted in the current method follows most closely the matrix procedure used by Leigh (Reference 9) wherein the iteration is a consequence of the solution of a set of linear and nonlinear algebraic relations with the

*Connected cubics were originally chosen (Reference 3), but connected quadratics have proven to be better behaved for highly blown boundary layers and with little or no loss in accuracy for less severe problems.

**As pointed out by Dorodnitsyn (Reference 7) differential procedures can be considered within this framework since they can be considered to employ Dirac delta weighting functions.

nonsimilar terms represented by quadratic finite difference relations). Whereas a special successive approximation procedure was used by Leigh, the general Newton-Raphson technique is used in the present procedure. This technique results in linearized coupling between all relations required to characterize the boundary layer, and thus assures a more rapid and stable iterative convergence.

In the general Newton-Raphson procedure, the nonlinear equations (the boundary-layer conservation equations and some of the boundary conditions) are linearized with respect to the primary dependent variables, and the errors introduced by the linearization are driven toward zero by iteration. This yields a matrix of equations of the form

$$\sum_j \frac{\partial E_n}{\partial V_j} \Delta V_j = - \text{ERROR}(E_n) \quad (1)$$

where E_n represents the n^{th} equation, V_j signifies the j^{th} primary dependent variable, $\text{ERROR}(E_n)$ represents the error in the n^{th} equation resulting from the previous iteration, and ΔV_j is the correction to be added to the variable V_j for the next iteration. The procedure thus requires an inversion of the matrix of derivatives $\partial E_n / \partial V_j$ to determine the ΔV_j . An elaborate system of tests are performed to determine a damping factor which is then applied uniformly to all corrections.

The BLIMP program contains approximately 5,000 instructions. The number of nodal points and the number of elements are the most critical dimensioned variables, in regard to both storage requirements and computational speed. Two versions currently exist: BLIMP1 is dimensioned for seven nodal points, five elements plus electrons, 30 species, and 20 streamwise stations; whereas BLIMP2 is dimensioned for 15 nodal points, seven elements plus electrons, 60 species, and 40 streamwise stations. BLIMP1 fits on the Univac 1108 without overlay, but requires an efficient overlay on most 32,000 word machines, while BLIMP2 requires the same overlay on the Univac 1108.

The BLIMP program takes two to three seconds per iteration on the Univac 1108 computer for a 7 node, 5 element, 30 species problem. The number of iterations required differs substantially according to the severity of the problem (the nonlinearity introduced by the chemistry events) and the first guesses. Typically 10 to 20 iterations are required for stagnation point

solutions involving complex chemistry starting with built-in, uninspired first guesses,* while downstream solutions require 3 to 6 iterations depending upon streamwise spacing. Thus a solution for a stagnation point plus 12 additional stations (this is sufficient to go around most bodies) would typically require 60 to 80 iterations corresponding to 2-1/2 to 3 minutes on the Univac 1108.

The BLIMP program has been checked out for the Apollo heat shield material in all of the applicable options. Solutions for a typical superorbital reentry trajectory are presented in Part II of this series of reports and are summarized in Section 6.4. Results for a 50,000 feet per second trajectory are also presented in Section 6.4. The BLIMP program has also been used extensively for the ablation of carbon in air (e.g., Ref. 10). Solutions have been generated for a number of additional problems such as teflon in air, graphite in a Venusian atmosphere, and injection of exotic transpirants such as hafnium tetrachloride and phosphorous pentoxide into air while maintaining surface equilibrium and steady-state energy balances over an ablating carbon surface.

2.2 CHARRING MATERIAL ABLATION (CMA) PROGRAM

The CMA program predicts the temperature and density histories of a thermally decomposing material exposed to a hyperthermal environment which supplies heat and which may chemically erode the material surface. The theoretical analysis, finite-difference solution procedure, and program characteristics are presented in detail in Reference 2 and are summarized in Reference 1. A user's manual is available as Reference 11.

Heat and mass transfer within the charring ablator is considered to be one-dimensional, but the thermal streamtubes are allowed to have arbitrary cross-sectional area. A general model for in-depth decomposition is considered. In one option detailed surface thermochemistry is considered, including selected rate-controlled reactions, and liquid-layer removal and mechanical spallation are taken into account through the use of a fail temperature for each candidate surface material.

The complex phenomena associated with the decomposition of the virgin material into a char and a pyrolysis gas are considered to be represented

*Typically 4 or 5 iterations are required for equivalent compressible non-reacting boundary layer problems.

by the conventional "simple physics" model

virgin plastic \rightarrow char + pyrolysis gas (2)

The virgin material is permitted to decompose while considering parallel Arrhenius type rate laws for three different constituents. The pyrolysis gases which form are considered to be in thermal equilibrium with the char, but no further chemical reactions with the char are permitted until the surface is reached. Cracking or other chemical reactions involving only the pyrolysis gases may be simulated with an appropriate gas enthalpy-temperature relation. However, coking of the pyrolysis gas to deposit carbon on the char is not permitted.

The CMA program permits up to eight different backup materials of arbitrary thicknesses. The back wall of the composite material may transfer energy by convection and radiation or may be insulated. Three options exist for the ablating surface boundary condition when CMA is operated as a main program:

- Option 1 - Transfer-coefficient model for convection-radiation heating with coupled heat and mass transfer considering detailed surface chemistry events.
- Option 2 - Specified surface temperature and surface recession rate
- Option 3 - Specified radiation view factor and incident radiation flux, as functions of time, for a stationary surface.

Any combination of these options may be used for a single computation. Option 1 is used when it is desired to predict ablation rates and surface temperatures as well as in-depth response. This option utilizes tabular data supplied by the ACE program (see Section 2.3) and is discussed in Section 2.4. Option 2 is useful for evaluating in-depth thermocouple data. Option 3 is appropriate to cooldown after termination of convective heat input and is often useful in conjunction with Options 1 and 2.

In another configuration, the program may be coupled to the boundary layer integral matrix procedure (BLIMP). In this arrangement, the total assembly is designated the CABLE program and is described in Section 2.5 below.

Material properties such as thermal conductivity, specific heat, and emissivity are input as functions of temperature for virgin plastic and char.

For partially decomposed material, the program performs an appropriate averaging to determine effective material properties.

An implicit finite difference solution procedure is employed in the CMA program. The following principles of differencing and nodal sizing are employed:

(1) The nodes have a fixed size. This avoids the slight additional computation complexity of shrinking nodes, and more importantly, makes principle (2) below easier to satisfy, in addition to preserving a useful nodal spacing throughout the history of a given problem.

(2) Since the nodes are fixed in size, not all of them can be retained if the surface of the material is receding due to chemical or mechanical erosion. From time to time a node must be dropped, and experience shows that it is much more preferable to drop nodes from the back (nonabating) face of the material rather than from the front face. This means that the nodal network is "tied to the receding surface," and that material appears to be flowing through the nodes. This involves a transformation of the differential equations to a moving coordinate system and somewhat complicates the algebra of the difference equations modeled on these differential equations. Disposing of nodes from the front surface, however, often leads to undesirable oscillations.

(3) The difference forms of derivatives are kept simple and are formed so as to provide a direct physical analog of the differential event leading to the derivative. This approach may be contrasted to those approaches which seek elaborate difference approximations to derivative expressions. Experience shows that the scheme adopted here, while sometimes at a minor disadvantage in accuracy, greatly simplifies the attainment of a major objective: a difference scheme which conserves energy and mass. Many of the more elaborate difference schemes fail to meet these "simple" but crucial conservation criteria, and hence frequently converge to erroneous or spurious solutions.

(4) The difference equation for energy is formulated in such a way that it reduces to the difference equation for mass conservation when temperatures and enthalpies are uniform. Any lack of consistency between the energy and mass equations complicates, and may entirely defeat, convergence to a meaningful result.

(5) The difference energy equations are written to be "implicit" in temperature. That is, all temperatures appearing are taken to be "new" unknown temperatures applicable at the end of the current time step. It is well established that implicit procedures are generally more economical than explicit procedures, at least for the majority of ablation problems of interest in the current work.

(6) In contrast to point (5), the decomposition relations are written as "explicit" in temperature. To implicitize temperature in these highly nonlinear equations necessarily involves either a time-consuming iteration procedure or an elaborate linearization.

(7) Since experience has shown that material decomposition rates are strongly dependent on temperature, it is highly desirable to perform the mass balance operations in a different, tighter network than that used for the energy balance equations. For greatest generality and utility, the number of these mass balance "nodelets" per energy balance "node" are freely selectable.

The storage requirements for the CMA program depend strongly upon the coupling mode in use. Coupling to a film coefficient model for the surface energy balance (Option 1) involves considerable table storage, hence the program barely fits a 32,000-word machine with full table sizes adequate to treat a wide variety of problems. In certain cases a reduction in table sizes will allow the program to fit on a smaller machine. As a subroutine to the CABLE program or with use of Option 2 or Option 3, the need for storing extensive boundary condition tables is eliminated. In these cases, the CMA program requires less than 8,000 words of storage.

Option 2 has been used extensively without difficulty in the evaluation of material thermal properties models from in-depth thermocouple data. A study of the Apollo material thermal properties model is reported in Part II of this series of reports. A typical result from this study is presented in Section 6.2. Experience to date with Option 1 is discussed in Section 2.4.

2.3 AEROTHERM CHEMICAL EQUILIBRIUM (ACE) PROGRAM

The ACE program solves for equilibrium chemical composition for a variety of open or closed systems of arbitrary chemical composition. The ACE program is an outgrowth of the chemistry subroutines of the BLIMP program which, in turn, can trace their origin to the Equilibrium Surface Thermochemistry (EST)

program (Ref. 12). The ACE program was developed as a byproduct of the current effort and, as a consequence, a comprehensive user's manual does not exist. However, the ACE program has been used extensively in the Apollo material studies presented in Part II of this series of reports and for this reason the characteristics of the program are summarized in this section. The equations which are solved, the solution procedure which is utilized, and the program characteristics are described in Reference 5 and are summarized in Reference 1.

The ACE program has the following major options:

1. Evaluation of chemical state for assigned pressure, elemental composition of several component mixtures which can be defined arbitrarily, and either enthalpy, entropy, or temperature
2. Solution of oblique shock relations to provide the state of the gases downstream of the shock and the isentropic stagnation state.
3. Calculation of surface mass balances to determine a relationship between normalized char recession rate, normalized pyrolysis gas rate, surface temperature, and pressure while considering equilibrium between the char and gases adjacent to it or while considering selected rate-controlled surface reactions.

All of these options are formulated for completely general chemical systems. Consideration of any molecular, atomic, ionic, or condensed species requires only the inclusion of the basic thermodynamic data appropriate for that species. These data are obtained, for example, from the JANAF Thermochemical Data Tables and include heat of formation and curve fit constants for entropy and specific heat.

Not too unlike the BLIMP program, the ACE program uses general Newton-Raphson iteration. Very elaborate convergence damping and rescue procedures have been developed over the period of years with a result that the program is very reliable. The solution procedure is discussed in some detail in Reference 5.

For most options a rather complete state of the system is generated which includes compositions, thermodynamic and transport properties, and property and composition derivatives (available as a consequence of the Newton-Raphson solution procedure). The surface state option provides additional information as discussed below.

The surface state option of the ACE program contains a number of features which make it useful in the analysis of ablation data.* In the first place, one does not have to choose a priori the surface species. For example, in the case of the Apollo material, the program will determine from the surface equilibrium relationships whether the char surface is SiO_2^* , C^* , SiC^* , Si^* or Si_3N_4^* . Secondly, each condensed species can be assigned a fail temperature above which it is not allowed to serve as the surface. This capability can be used to represent mechanical removal of a species which may want to precipitate out but which has poor bonding characteristics or a species which wants to appear above its melt temperature. Thirdly, it is possible to chemically isolate species or component gas mixtures from the system or to consider rate-controlled surface reactions or surface-catalyzed homogeneous reactions. In Part II of this series of reports, these latter two capabilities are used in conjunction with each other to develop a rate law for the mechanical removal of silica for the Apollo heat shield material based on a correlation of ground test data. A fourth major capability of the ACE program is that it permits consideration of unequal diffusion coefficients as well as unequal heat and mass-transfer coefficients through an application of the same approximation for binary diffusion coefficients utilized in the BLIMP program. This approach is developed in Reference 13. A principal limitation of the ACE program is that the surface is required to consist of a single condensed species. Thus, the surface of the Apollo material might be C^* with SiO_2^* and/or SiC^* failing, but C^* and SiO_2^* , say, cannot serve simultaneously as the surface material.

The surface state options of the ACE program provide char recession rate normalized by a mass-transfer coefficient, and other information needed to perform an energy balance on the surface of a charring ablation material, as a function of pyrolysis gas rate normalized by the same mass-transfer coefficient, surface temperature, and pressure. It thus does not by itself constitute an ablation prediction tool. In the first place, it is necessary to specify the mass-transfer coefficient and this cannot be done precisely without solving the boundary-layer equations. Secondly, the determination of surface temperature requires the solution of a surface energy balance. One procedure which is used for ablation predictions is to generate surface state solutions with the ACE program in the form of punched card output. This is then used as input to the CMA program (Option 1) which performs the surface energy balance. This is still only a partial theory, however, in that the

*These same features are in the surface chemistry options of BLIMP.

transfer coefficients must still be specified. These can be obtained from correlations of boundary layer solutions obtained, for example, from the BLIMP program. On the other hand, the BLIMP program operated in its steady-state energy balance option and BLIMP coupled with CMA through the CABLE program constitute complete coupled theories. The CMA/ACE approach is described in Section 2.4, whereas the CABLE program is described in Section 2.5.

In spite of the fact that the ACE program was developed as a byproduct of the present study, it has through utilization become a very reliable program, seldom failing to yield a valid solution for any of its options. However, further documentation and cleanup is required before the program can be considered fully operational.

A systematic study of ground and flight test data for the Apollo heat shield material using the ACE program as the principal computational tool is presented in Part II of this series of reports. Some representative solutions are also presented in Section 6.3 of this summary report.

2.4 CMA/ACE COUPLING PROCEDURE

The CMA/ACE approach, described in Reference 1, provides an economical means for obtaining transient charring ablation predictions while considering detailed surface thermochemical events. The CMA and ACE programs are mechanically decoupled, punched card output from ACE being used as input to the CMA program. However, the final result is effectively a coupled solution. The ACE data provides the surface mass balance and surface equilibrium (or non-equilibrium) constraints while the CMA program provides the pyrolysis gas rate and conduction term and solves the surface energy balance. However, as mentioned previously, this is a partial and thus approximate coupled procedure for the following reason. In the CMA/ACE approach the user must specify a nonablating heat-transfer coefficient, a relation between heat- and mass-transfer coefficients, and a blowing reduction relationship.

Fully coupled (complete) solutions can be generated for some problems by the following approach. First, the BLIMP program is run with no injection for the flight conditions of interest and with various char and pyrolysis-gas injection rates covering the anticipated ranges of these parameters. The latter are correlated to determine a blowing reduction law and a relationship between heat- and mass-transfer coefficients, while the former provides non-ablating heat-transfer coefficients. This information is then used as input to the CMA program, together with the tabular ACE data. Spot checks of the

CMA results can then be made by running the BLIMP program with char and pyrolysis gas injection rates and surface temperatures assigned at the values generated by the CMA solution, and comparing the resulting heat- and mass-transfer coefficients with those used in the CMA solution. This process can then be repeated if discrepancies in the transfer coefficients appear to warrant such action.

This process can be made to duplicate the results of fully coupled CABLE solutions (which couples BLIMP and CMA directly) at the stagnation point for assumed equal diffusion coefficients, but is only approximate for downstream stations or when unequal diffusion effects are considered. The reason for this is that the CMA and ACE programs are based on a single mass-transfer coefficient, $\rho_e u_e C_{M_i}$, whereas in nonsimilar or unequal diffusion problems the $\rho_e u_e C_{M_k}$ will in general differ for each chemical element. One of the primary purposes of the approximation for unequal diffusion coefficients (Refs. 4 and 13) which is employed in the ACE program is to redefine the driving potential for mass transfer such that the $\rho_e u_e C_{M_k}$ tend to become equal. The success of this operation has never been thoroughly tested, but preliminary BLIMP results (Ref. 10) for ablation of carbon in air are very encouraging, at least for that three-element system. In a like manner, the $\rho_e u_e C_{M_k}$ cannot be expected to always be equal around the body, even for assumed equal diffusion coefficients, as a consequence of nonsimilar mass injection distributions.

The coupled computation procedure constituted by the CMA and ACE programs has been applied to a wide variety of materials of technical interest with excellent to poor correlation depending upon the particular material and boundary conditions. Any discrepancies between predictions and data have been clearly attributable to effects not considered in the calculation (but available in the programs), effects not considered in the programs, or to ill-judged boundary conditions or material properties. The approach is fully checked out and operational for the physical and chemical models currently employed. Occasionally an iteration stop is encountered because the surface energy balance fails to converge, but this can usually be traced to incomplete ACE tables or other input consideration and can be easily corrected.

Computation time depends, of course, on the problem being computed, but experience to date indicates that CMA computations run in roughly 1/3 of real time for "typical" charring material problems for machines of the IBM 7094 speed class. Predictions generated for recent Apollo superorbital reentry trajectories are presented in Part II of this series of reports and summarized in Section 6.7 of the present report.

2.5 COUPLED ABLATOR/BOUNDARY LAYER/ENVIRONMENT (CABLE) PROGRAM

The Coupled Ablator/Boundary Layer/Environment (CABLE) program is a computational procedure which couples the one-dimensional transient response of a charring heat shield material to a chemically reacting two-dimensional laminar boundary layer. The CABLE program incorporates subroutine versions of the BLIMP program (described in Section 2.1) and the CMA program (described in Section 2.2). The features of the CABLE program and the mechanics of coupling are discussed in this section, while the coupling procedure is demonstrated further by an Apollo superorbital reentry problem in Section 6.8.

All of the features of the BLIMP and CMA programs pertinent to the coupled problem are retained in the CABLE program. The models employed in the CABLE program are summarized in Table I. The operational status of the various aspects of the computational procedure are also summarized therein. It can be seen that most considerations are fully operational, including all aspects of the in-depth response of the ablating surface material and the nonablating backup materials. Certain aspects of the boundary-layer solution cannot be considered fully operational until such time that the procedure is checked out for the wide variety of materials, environments and flight conditions for which it is presumably applicable.

The CABLE solution procedure is virtually the same as reported in Reference 1. As discussed therein, several approaches for coupling the boundary layer and charring ablation solutions were considered in the development of the CABLE program. The method which was finally adopted was selected on several bases: it makes use of options of existing programs which are well exercised and known to perform well, it avoids extrapolation of surface boundary conditions, and it avoids repeated (iterative) solution of the boundary layer and transient charring ablation response. The various other methods which were considered were inferior in one or more of these considerations. Furthermore, storage requirements and computational time are improved relative to most if not all of the other methods considered.

In the procedure which was adopted, the transient charring ablation solution is effectively the controlling program. The charring ablation solution at a given station proceeds noniteratively, calling the boundary-layer procedure as needed to supply the surface boundary condition. The complete transient history at each axial station is performed prior to advancing to the next axial station. This is accomplished by performing sets of nonsimilar boundary-layer solutions at the current station for a discrete array of times

TABLE I
COUPLED ABLATOR/BOUNDARY LAYER/ENVIRONMENT
(CABLE) COMPUTER PROGRAM

I BOUNDARY-LAYER-EDGE CONDITIONS		
<u>Phenomena</u>	<u>Model</u>	<u>Operational Status</u>
(a) Flight conditions	Transient or steady-state; local stagnation conditions and pressure distribution around the body are specified; program performs isentropic expansion around body	Fully operational
(b) Environmental gas	Arbitrary elemental and molecular composition	Fully operational
(c) Chemical state	General mixed equilibrium-frozen	See Item II (e)
(d) Incident radiation	Net radiant heat flux	See Item II (g)
II BOUNDARY LAYER		
(a) Boundary-layer type	Laminar nonsimilar with discontinuous mass injection	Fully operational
(b) Nature of solution	Numerical procedure capable of yielding accurate solutions	Fully operational; three to four place accuracy obtained with relatively few nodal points
(c) Body geometry	General planar or axisymmetric flow around blunt or sharp bodies; three-dimensional boundary layers can be approximated by use of axisymmetric analogy	Fully operational

TABLE I (Continued)

II BOUNDARY LAYER (Continued)		
<u>Phenomena</u>	<u>Model</u>	<u>Operational Status</u>
(d) Chemical system	Arbitrary elemental and molecular composition	Fully operational
(e) Chemical state	General mixed equilibrium-frozen with arbitrary heterogeneous (surface) reaction kinetics	Fully operational for equilibrium; some solutions have been obtained for partially frozen boundary layers with rate-controlled surface reactions or surface-catalyzed reactions
(f) Transport properties	Incorporates bifurcation approximations for unequal diffusion and thermal diffusion coefficients and approximations for mixture viscosity and thermal conductivity of the Sutherland-Wassilijewa type	Fully operational for equal diffusion coefficients; convergence can be slow and nonconvergences sometimes occur in problems with unequal diffusion coefficients due to inexact derivatives in the Newton-Raphson iteration procedure
(g) Radiation absorption and emission	Incident flux considered to pass through boundary layer without attenuation	Fully operational
III SURFACE PHENOMENA		
(a) Coupling considerations	The boundary layer and charring ablator solution fully coupled; transient solution at a given streamwise station completed before proceeding to next station	Solutions obtained only for Apollo heat shield material; further checkout is required before the coupling can be considered fully operational for all materials and environments for which it is presumably applicable

TABLE I (Continued)

III SURFACE PHENOMENA (Continued)	<u>Phenomena</u>	<u>Model</u>	<u>Operational Status</u>
(b) Chemical interactions	Chemical reactions between char, pyrolysis gas, and boundary-layer species allowed; these reactions are assumed to be in equilibrium except for specified rate-controlled reactions	Equilibrium fully operational; some solutions have been obtained for selected rate-controlled reactions	
(c) Mechanical removal mechanisms	Each candidate surface condensed phase material (e.g., SiO_2^* , C^* , SiC^*) assigned a fail temperature, above which that species cannot appear as the surface material (this is equivalent to specifying, for example, a zero liquid viscosity for SiO_2^* above its melt temperature)	Operational for those surface materials which have been considered	
IV IN-DEPTH RESPONSE OF EXPOSED (ABLATING) MATERIAL	(a) Class of materials	Any charring or noncharring material for which thermochemical data are available or can be estimated	Fully operational
(b) Geometry	One-dimensional conduction but area change due to material curvature taken into account in a generalized manner, with planar, cylindrical, and spherical geometries as special cases	Fully operational	
(c) Thermal properties	Temperature dependent	Fully operational	
(d) Pyrolysis kinetics and subsequent internal chemical events	Pyrolysis can be specified by 3 independent kinetic reactions; thermal equilibrium between the char and pyrolysis gas assumed; formulation consistent with general pyrolysis-gas cracking, the user employing pyrolysis-gas enthalpy as function of temperature; char density buildup due to coking not calculated	Fully operational	

TABLE I (Concluded)

IV	IN-DEPTH RESPONSE OF EXPOSED (ABLATING) MATERIAL (Continued)		<u>Operational Status</u>
	<u>Phenomena</u>	<u>Model</u>	
	(e) Numerical technique	Implicit finite-difference, except that gas generation is partially explicit	Fully operational
	(f) Other numerical considerations	Variable grid spacing with nodelets used in decomposition zone. Nodes dropped from rear of ablation material	Fully operational
V	IN-DEPTH RESPONSE OF BACKUP MATERIALS		Fully operational
	General	Several noncharring materials with variable thermal properties are allowed, with interfacial contact resistance (including air gaps) between materials, and variable rear surface boundary conditions	

(θ_i), normalized pyrolysis-gas mass flow rates (\dot{m}_g^*), and normalized char mass flow rates (\dot{m}_c^*) (or surface temperatures, T_w , when $\dot{m}_c^* = 0$) which bracket the current values for these parameters. Calculations for intermediate times and intermediate values of \dot{m}_g^* and \dot{m}_c^* (or T_w) are then performed by interpolation as they are needed for the charring ablation solution. (It is significant that only those members of the \dot{m}_g^* , \dot{m}_c^* (or T_w) array needed to contain current values are considered, and that at any instant, these are required for only a pair of times.)

When the charring ablation solution proceeds to the point where the \dot{m}_g^* or \dot{m}_c^* (or T_w) reaches a currently bracketing value, the BLIMP program is called upon to provide solutions for the next entry of the parameter which is about to be exceeded. Whenever a new \dot{m}_g^* or \dot{m}_c^* is being considered, the BLIMP program is also called upon to generate surface equilibrium calculations to determine the surface temperature at which ablation would commence so that the CMA program will be able to move from T_w to \dot{m}_c^* (or vice versa) as an independent parameter. When time θ_i is approached, a CMA solution is performed at precisely that time and a BLIMP solution is generated for the resulting T_w , \dot{m}_g^* and \dot{m}_c^* . These then serve as the coupled charring ablation and boundary layer solutions at that time. The BLIMP program is then called upon to generate solutions for the next time, θ_{i+1} , for the currently bracketing values of \dot{m}_g^* and \dot{m}_c^* (or T_w if nonablating) and to determine the ablation temperatures for the current \dot{m}_g^* and new time. These solutions are placed over those for time θ_{i-1} (which are no longer needed) by a tape flip-flop procedure.

The coupling procedure was illustrated schematically in Reference 1 and will be demonstrated further in an Apollo superorbital reentry problem presented in Section 6.8.

Since the writing of Reference 1, the major improvement of CABLE has been the vastly improved reliability of the BLIMP subroutine. During the early portion of a superorbital Apollo reentry, mass injection rates typically become very large and the boundary layer can be blown off the surface. (This will be illustrated in Section 6.8). Also, complex chemistry and mechanical removal processes are taking place. However, as will also be demonstrated in Section 6.8, the BLIMP program is able to perform such calculations with the requisite 100 percent reliability, primarily as a result of the extensive convergence damping procedures which have been developed for BLIMP. A second major advance has been the development of a CABLE restart capability. The information needed for restart is stored on tape after every final boundary layer solution at a given time (i.e., the BLIMP solution corresponding

to the actual T_w , \dot{m}_g^* and \dot{m}_c^* at that time which were computed by CMA from an interpolation of BLIMP solutions).

The computational time is dependent upon the type of problem under consideration and the number of \dot{m}_g^* , \dot{m}_c^* , T_w and θ_i which enter the problem. The CABLE program spends most of its time in BLIMP performing boundary layer solutions. A minimum of 6 and on the average probably about 10 boundary layer solutions are required for each time step $\Delta\theta_i$, each boundary layer solution taking 15 to 20 seconds on the Univac 1108 computer. A nonsimilar solution around the Apollo heat shield for a complete superorbital trajectory would necessitate about 15 time steps and 10 streamwise stations.

SECTION 3

ANALYSIS AND COMPUTATIONAL PROCEDURE FOR SOLUTION OF INCOMPRESSIBLE TURBULENT BOUNDARY LAYERS (SAINT PROGRAM)

3.1 GENERAL

The integral matrix solution procedure which was first developed for the laminar BLIMP code and is summarized in Section 2.1 has been applied to the solution of planar constant property nonsimilar turbulent boundary layers. The present application represents a simplification with regard to the environmental generality embodied in the laminar procedure (general equilibrium chemistry, multicomponent diffusion, compatibility with the CMA program as a surface boundary conditions, etc.), but has been developed with the intention of adding these features later. In view of this intended final result, the arguments presented in Section 2.1 relative to minimization of the number of entries into the conservation equations and maximizing streamwise step size are still valid; hence, basically the same solution procedure has been employed.

The general approach for describing the turbulent boundary layer includes dividing the flow into two layers: a law of the wall region and a wake region. The turbulent "equation of state" used is simply the definition of an eddy viscosity, which relates the Reynolds' stress term to the mean motion. Techniques for describing eddy viscosity in the wall and wake regions are quite different and a matching or blending of the two regions is required. The boundary layer equations and turbulent model are summarized in Section 3.2, the solution procedure is summarized in Section 3.3, and the resulting computer code, Strip Analysis of Incompressible Nonsimilar Turbulent boundary layers (SAINT), is described in Section 3.4. These subjects are covered in detail in Part IV of the present series of reports, together with a number of sample solutions.

3.2 BASIC EQUATIONS AND TURBULENT MODEL

3.2.1 General Equations of Motion

The equations of motion for a turbulent boundary layer are typically derived from the Navier Stokes equations by decomposition of the velocity field into mean and fluctuating components, time averaging, and making appropriate order of magnitude approximations. These operations result in the global continuity equation

$$\frac{1}{r_o^\kappa} \frac{\partial \rho u r_o^\kappa}{\partial s} + \frac{\partial \rho v}{\partial y} = 0 \quad (3)$$

and the momentum equation

$$\rho u \frac{\partial u}{\partial s} + \rho v \frac{\partial u}{\partial y} = - \frac{dP}{ds} + \frac{\partial}{\partial y} \left(\mu \frac{\partial u}{\partial y} - \overline{\rho u'v'} \right) \quad (4)$$

where conventional nomenclature has been employed (see List of Symbols). Triple correlations and streamwise derivatives of turbulent correlations have been dropped in these equations. Equations (3) and (4) would allow calculation of u and v in a constant property boundary layer for the proper boundary and initial conditions if the turbulence term were known. The assumptions made regarding this turbulence term provide the greatest differences between the turbulent boundary layer techniques available today.

There are many choices available to describe the "Reynolds' stress" term $\overline{\rho u'v'}$ which appears in Equation (4). One approach which has met with success for many types of flows is the eddy viscosity description of turbulence. In this approach, the turbulent stress is related to the mean velocity field through the relation

$$\overline{\rho u'v'} = \rho \epsilon \frac{\partial u}{\partial y} \quad (5)$$

where ϵ is the eddy viscosity. Since this approach lends itself to the more complex systems which will eventually be analyzed with this program, it will be adopted here. The momentum equation becomes

$$\rho u \frac{\partial u}{\partial s} + \rho v \frac{\partial u}{\partial y} = - \frac{dP}{ds} + \frac{\partial}{\partial y} \left[\rho (\epsilon + \nu) \frac{\partial u}{\partial y} \right] \quad (6)$$

The eddy viscosity can be related to global parameters of the flow such as δ^* in the outer portion of the boundary layer, and is typically described by a "law of the wall" in the inner portion of the boundary layer. The procedures adopted for each of these regions are discussed in the following sections.

3.2.2 Law of the Wall Region

In the law of the wall region, the boundary layer flow can be thought of as completely one-dimensional. That is, the mean flow field properties can

be described entirely in terms of the wall state, wall fluxes, thermodynamic and transport properties of the fluid, and the normal coordinate y . Since the streamwise coordinate does not enter the solution, the problem becomes a one-dimensional initial value problem. Utilizing this information in the continuity and momentum equations results in the relation

$$\rho_w v_w u = \rho(v+\epsilon) \frac{du}{dy} - \tau_w \quad (7)$$

For flows over an impermeable wall with constant properties, this reduces to

$$\rho(v+\epsilon) \frac{du}{dy} = \tau_w \quad (8)$$

or

$$\tau = \tau_w \quad (9)$$

indicating that shear can be considered constant in the law of the wall region. For incompressible flows with injection, it is seen that shear varies with the injection rate and local velocity, i.e.,

$$\tau = \tau_w + \rho_w v_w u \quad (10)$$

Because of the current lack of understanding of turbulent mechanisms, "theoretical" predictions of the variation of turbulence near the wall must rely on empirical input into relations having some phenomenological dependence. Because of the generality of the ultimate goals of this analysis and of the desire to approximate the physical situations, certain prerequisites were established for the turbulent transport relations. These were:

- a. The relations must indicate a continuous variation of the turbulent transport properties from the wall to the fully turbulent region.
- b. The relations must be generally applicable to mass, momentum, and energy transport.
- c. The relations must be extendable to compressible real gas property flow.
- d. The relations should be suitable for transpired and untranspired boundary layers with little or no modification of form.

Other investigations (Refs. 14 and 15) have shown that a mixing length hypothesis sufficiently describes the turbulent shear in the wall region, both with and without injection. As a consequence of this apparent generality of the mixing length approach, it was adopted for the present studies.

The basic mixing length postulate can be expressed as

$$\overline{\rho u'v'} = \rho \ell^2 \left(\frac{du}{dy} \right)^2 = \rho \epsilon \left(\frac{du}{dy} \right) \quad (11)$$

where the mixing length, ℓ , is a combination of various correlations, but retains some relationship to the scale of turbulence. Using physical logic and some intuition, a differential equation governing the development of the mixing length for the law of the wall region was postulated. It is

$$\frac{d\ell}{dy} = (Ky - \ell) \frac{\sqrt{\tau/\rho}}{(y_a^+)^{\nu}} \quad (12)$$

where y_a^+ is a constant of proportionality and K is the conventional Prandtl mixing length constant.* These have been shown in Reference 15 to be invariant for a wide variety of flow conditions at $y_a^+ = 11.83$ and $K = 0.44$. This differential equation is linear and of first-order; therefore it can be integrated in general form to yield

$$\ell = K \left[y - \frac{\int_0^y \int_0^{y'} P dy'' dy'}{\int_0^y P dy'} \right] \quad (13)$$

where

$$P = \frac{\sqrt{\tau/\rho}}{(y_a^+)^{\nu}} \quad (14)$$

*This equation satisfies the Reichardt-Elrod criteria at the wall, Prandtl's expression for small y , and Rotta's result for large y (see Part IV of this series of reports).

For the special case of constant properties and zero injection (constant shear), this becomes

$$\ell = \frac{Kv}{u_\tau} \left\{ y^+ - y_a^+ \left[1 - \exp\left(\frac{-y^+}{y_a^+}\right) \right] \right\} \quad (15)$$

where

$$u_\tau = \sqrt{\frac{\tau_w}{\rho}} \quad (16)$$

$$y^+ = \frac{yu_\tau}{\nu} \quad (17)$$

Due to the simplicity and apparent physical adequacy of this model, Equation (12) has been adopted for this analysis.

3.2.3 Wake Region

The wake region comprises the outer 80 to 90 percent of the boundary layer. It is two-dimensional in nature and therefore provides the mechanism for transmitting nonsimilar effects (the wall region being considered one-dimensional). Perhaps the most interesting feature of this region of the boundary layer is that eddy viscosity appears to be nearly constant here. Clauser (Ref. 16) was able to relate the eddy viscosity to edge velocity and a length scale, i.e.,

$$\frac{\epsilon}{u_e \delta^*} = K_c \quad (18)$$

with $K_c = 0.018$ for a great quantity of experimental data taken in equilibrium flows. Equilibrium in this sense refers to the requirement of the parameter $\frac{\delta^*}{\tau_w} \frac{dP}{ds}$ to be constant for equilibrium to exist. The expression above has proved accurate and useful for many applications and is used in the present analysis.

Primarily for convenience and generality of results, the governing equations for the wake region are typically transformed to a new dimensionless coordinate system which allows similar solutions for certain sets of boundary conditions and makes a numerical solution easier to generalize. One popular

transformation is the Levy-Lees transformation. For strictly turbulent flows, a new transformation which normalizes the y coordinate by a parameter which grows roughly as the turbulent boundary layer thickness was thought more appropriate. Such a transformation is

$$\left. \begin{aligned} \xi &= \int_0^s \rho_e u_e r_o^\kappa ds \\ \eta &= \frac{1}{\delta \alpha_H} \int \frac{\rho}{\rho_e} dy \\ \delta &= \frac{\xi}{\rho_e u_e r_o^\kappa} \\ f &= f_w + \frac{1}{\rho_e u_e \delta} \int_0^y \rho u dy \\ f_w &= - \frac{1}{\rho_e u_e \delta r_o^\kappa} \int_0^s \rho_w v_w r_o^\kappa ds \end{aligned} \right\} \quad (19)$$

The simplifications for constant density flow are obvious. For this special case, the governing momentum equation becomes

$$ff'' + \frac{1}{\alpha_H} \left[\frac{(\epsilon + \nu)}{u_e \delta} f'' \right]' + \frac{\theta}{2} (\alpha_H^2 - f'^2) = \alpha_H f' \frac{\partial (f'/\alpha_H)}{\partial \ln \xi} - f'' \frac{\partial f}{\partial \ln \xi} \quad (20)$$

where the prime denotes differentiation with respect to η .

The parameter $\alpha_H(\xi)$ is determined by requiring the velocity ratio u/u_e to have a value, say \bar{C} , at a specific value of η , say $\eta_{\bar{C}}$. Thus

$$\alpha_H = \frac{f'}{\bar{C}} @ \eta_{\bar{C}} \quad (21)$$

The surface boundary conditions neglecting slip and including mass injection are given by

$$\left. \begin{aligned} f|_w &= f_w(\xi) \\ f'|_w &= 0 \end{aligned} \right\} \quad (22)$$

whereas the boundary layer edge conditions are

$$\left. \begin{aligned} f' \Big|_e &= \alpha_H \\ f'' \Big|_e &= 0 \end{aligned} \right\} \quad (23)$$

3.3 SOLUTION PROCEDURE

The solution of the transformed turbulent boundary layer equations presented in Section 3.2 utilizes an integral matrix method patterned after the method developed for the BLIMP program. Since this approach has already been summarized in Section 2.1 of this report and presented in detail in Reference 3 it will be only briefly reviewed here as it relates to the current development.

In this approach, the boundary layer is divided into a number of strips in the streamwise direction. The momentum equation (20) is first reduced to a set of ordinary differential equations in the boundary-layer normal direction at a given streamwise station by replacing the streamwise derivatives by quadratic finite difference relations (this expresses the derivatives at the current streamwise station in terms of unknown values at the current station and known values at the two streamwise stations immediately upstream). At a given streamwise station, the momentum equation is integrated with a step weighting function over each strip.*

The integral equation for mixing length (13) is solved by representing $P(y)$ across the strips in an approximate manner and forming a simple recursion formula for l_i

$$l_i = K(y_i - L_i) \quad (24)$$

where

$$L_i = \frac{L_{i-1}}{\left(\frac{P_i + P_{i-1}}{2} \right) \Delta_i} + \frac{1}{a} \left[D(d) - e^{c^2 - d^2} D(c) \right] \quad (25)$$

* In Reference 17, the momentum equation is solved in differential form. The two approaches are equivalent in accuracy and stability. The integral approach adds slight complexity to the incompressible boundary layer problem, but affords great algebraic simplification in chemically-reacting boundary layer problems (see Ref. 3), the ultimate goal of this effort.

with

$$\left. \begin{aligned} \Delta_i &= Y_i - Y_{i-1} \\ a &= \frac{P_i - P_{i-1}}{2\Delta_i} \\ c &= \frac{P_{i-1}}{2a} \\ d &= a\Delta_i + c \end{aligned} \right\} \quad (26)$$

and $D(\)$ the Dawson Integral* of the quantity in brackets.

The primary dependent variables are taken to be α_H and the f_i , f'_i , f''_i , and f'''_i at each strip boundary i . The f_i , f'_i , and f''_i are related to their derivatives by truncated Taylor series expansions. This has the net effect that f'_i across the boundary layer is represented by series of connected cubics with continuous first and second derivatives at the junction points (strip boundaries). These Taylor series expansions, which are linear with respect to the primary dependent variables, form a very sparse matrix which has to be inverted only once for a given problem to express the nonlinear equations and boundary conditions at the current streamwise station in terms of the f'_i , α_H , f'_w , f''_w , and f'_e . These remaining equations are then solved by general Newton-Raphson iteration. Uniform damping of all corrections based upon limits allowed on corrections for f'_w and α_H is employed to add stability to the convergence procedure. The solution at a given streamwise station is considered converged when the errors in all equations are reduced to acceptably low values. The solution then moves to the next streamwise station.

3.4 THE SAINT BOUNDARY LAYER PROGRAM

The SAINT program generates velocity profiles and boundary layer parameters (drag coefficient, momentum and displacement thicknesses, shape factor, etc.) for the flow model described in the previous sections. Nonsimilar terms are retained in general; however, similar solutions within the context of the transformation outlined in Section 3.2.3 can also be obtained. At present,

* $D(x) = e^{-x^2} \int_0^x e^{y^2} dy$

only incompressible, single component flows with or without injection can be solved. Turbulent intermittency can be considered; however, universally successful formulations of an intermittency function have not been found (Ref. 17). Thus, intermittency has been neglected for all problems run to date.

The program requires a specification of the nodal network; streamwise stations at which a solution is desired; and edge velocity, velocity gradient and injection velocity at each of these stations. It also requires values for kinematic viscosity, intermittency factor, the Clauser parameter, $\epsilon/u_e \delta^*$, and the two wall law constants y_a^+ and K . The program will accept an initial profile at the first station or will generate a similar profile.

The program can be used to solve laminar problems by setting the Clauser parameter, $\epsilon/u_e \delta^*$, equal to zero. Care must be exercised in using this option, however, since the coordinate transformation is improper for laminar similar problems.

The program is presently dimensioned for up to 15 nodes in the boundary layer and 50 axial stations. Core requirements are approximately 30,000 octal words.

Typical boundary layer solutions for blown and unblown boundary layers and comparisons with experimental data are presented in Part IV of this series of reports.

3.5 CONCLUDING REMARKS

The incompressible turbulent boundary layer analysis and computer program described here have been formulated with the intention of extending to compressible, multicomponent, reacting flows. The incompressible version thus contains features which were included specifically for the final version. The present version has been developed primarily as a test bed to study turbulent models, the status of which is still subject to improvement. Therefore, the program has also been written in such a manner that the governing equations for mixing length and wake eddy viscosity can be readily changed.

SECTION 4

ANALYSIS AND COMPUTATIONAL PROCEDURE FOR THE EVALUATION OF NONGREY RADIANT HEAT FLUX (RAD PROGRAM)

4.1 GENERAL

Procedures are presented for the prediction of radiation properties for and transport within a C-H-O-N elemental system. This system is considered to be representative of boundary layers adjacent to most ablating bodies. Local thermodynamic equilibrium is assumed to exist at all times. Molecular, atomic and ionic species are all considered with those which appear in the 3,000°K to 15,000°K temperature range (0.1 to 10 atm pressure range) being given primary consideration.

The radiation properties and transport models are reported in detail in Part III of this series of reports and are summarized in Sections 4.2 and 4.3 of the present report, respectively. A description of the resulting radiation transport code (RAD) is given in Reference 18 and summarized in Section 4.4.

4.2 ABSORPTION COEFFICIENTS OF THE BOUNDARY LAYER SPECIES

The spectral absorption coefficient for a plasma consisting of a mixture of elements is in general

$$\mu_\nu = \sum_{i=1}^{N_1} \mu_i^C(\nu) + \sum_{k=1}^{N_L} \mu_k^L(\nu) \quad (27)$$

where the first term represents the continuum contribution with the summation taken over all continuum transitions (N_1), and the second term represents the line contribution with the summation taken over all the lines (N_L). For the plasma conditions of interest, the important continuum transitions include atomic photoionization, photodetachment, free-free transitions, photodissociation, and molecular photoionization in approximately a decreasing order of importance. The atomic line transitions are very important. The molecular band systems can be important for some conditions.

4.2.1 Atomic and Ionic Continuum Transitions

In general, continuum contributions depend on the plasma state (to a satisfactory approximation) only through the populations of the absorbing

levels, viz.

$$\mu_i^C(\nu) = \sum_j N_{ij} \sigma_{ij}^C(\nu) \quad (28)$$

where N_{ij} is the number density of the absorbing level and $\sigma_{ij}^C(\nu)$ is its cross-section. The number densities are obtained from thermodynamic state calculations (e.g., ACE code). The cross-sections have been selected from quantum mechanical calculations and/or experiments appearing in the literature.

The photoionization and free-free cross-sections are from several sources. The tabulations of "effective cross-sections" presented by Wilson and Nicolet (Ref. 19) are used for all the atomic and ionic species except hydrogen. These tabulations are based on the quantum defect method which is approximate, but is the most reliable method available short of a detailed evaluation of the quantum mechanical equations. For hydrogen, classical cross-sections are utilized, small corrections due to quantum mechanical effects being neglected. Integral formulas are used in all cases to approximate contributions from the higher levels (principal quantum numbers greater than three). In the case of carbon, the integral formula of Biberman and Norman (Ref. 20) is used for all the excited levels, consistent with the tabulations of Reference 19.

4.2.2 Atomic Line Transitions

The absorption coefficients of the atomic line transitions depend on the plasma condition both through the population of the absorbing level and through the shapes of the lines. Thus,

$$\mu_{k(j)}^L(\nu) = \frac{\pi e^2}{mc} f_{k(j)} N_{ij} b_{k(j)}(\nu, T, P, x_1, x_2, \dots) \quad (29)$$

where $f_{k(j)}$ is the oscillator strength of the k^{th} line in the j^{th} series of lines and $b_{k(j)}(\nu, T, P, x_1, x_2, \dots)$ is the line shape and is a function of frequency and the plasma condition. The line shape obeys the normalization condition (omitting the explicitly written functional dependence on the plasma condition for brevity)

$$\int_0^\infty b_k(\nu) d\nu = 1 \quad (30)$$

but otherwise is free to take on a variety of functional forms depending upon the species involved and the broadening mechanism (or combination of mechanisms).

For the heavy atomic species, the dominant broadening mechanism is Stark broadening by electron impacts. Following Armstrong et. al. (Ref. 21) it is assumed that each multiplet can be treated as a line with a Lorentz shape, viz.

$$b_k(\nu) = \frac{\gamma_k^S/\pi}{(\nu-\nu_k)^2 + (\gamma_k^S)^2} \quad (31)$$

where ν_k is the frequency of the line center and γ_k^S is the Stark (half) half-width which is a function of the plasma condition. Corrections of Equation (31) due to J-splitting and effects due to ion perturbers are ignored.

The (half) half-widths for the important transitions in N, N+, O, O+, C and C+ are from the tabulations of Wilson and Nicolet (Ref. 19). They are based on the electron impact approximation and are in good agreement with a similar but less extensive tabulation given by Griem (Ref. 22).

The broadening mechanisms for atomic hydrogen require exceptional treatment. The Stark splitting of hydrogen lines is much greater than that of other spectra. Further, it is known that broadening caused by ion perturbers is not negligible compared to that caused by electron impacts (see Ref. 23). Thus, the Lorentz line shapes cannot be used. The line shapes in the core region of each of the important hydrogen lines are from the tabulations by Griem, Kolb and Shen (Ref. 23). The shapes of the wings are from asymptotic equations given by Griem (Ref. 22).

When the lines are weak or strongly overlapped, fully detailed evaluations of Equations (29) and (31) (or the appropriate line shape for hydrogen) and the second term of Equation (27) are often not required for the accurate evaluation of the properties of the lines. Integral formulas are available which convert the line contributions into equivalent continuum contributions, achieving a significant simplification. These have been used for the contributions from the high lines (upper principal quantum number greater than eight) and the high series lines (lower principal quantum number greater than three). In the first case, the photoionization thresholds are lowered in the spirit of a method suggested by Armstrong (Ref. 24). In the second case, a closed form equation suggested by Vorobyov and Norman (Ref. 25) is utilized.

Even for strong and/or isolated lines, a fully detailed evaluation of Equations (27), (29) and (31) is fortunately not required; rather, the line group approximation is utilized. The contributions from nearby lines are included, whereas those from distant lines are neglected. The frequency range of interest is divided into a number of frequency increments - 15 to 20 or thereabout which are not necessarily connected. Each one defines as a line group those lines which are centered within it. The line contributions at a frequency point within a frequency increment is obtained by summing over only those lines within its group. Again, a significant simplification results.

4.2.3 Molecular Band Transitions

The molecular band systems are treated as a psuedo continuum, rather than as groups of individual bands, to simplify the model. The bands within each band system are smeared according to the scheme

$$\bar{\mu}_v = \frac{\int_{\Delta v} \mu_v dv}{\Delta v} \quad (32)$$

where the Δv are selected such that $\bar{\mu}_v$ varies smoothly. The "bandless model" obtained in this fashion is essentially the same as that proposed originally by Meyerott et. al. (Ref. 26) and used more recently by Biberman and Mnatsakanyan (Ref. 27). It is felt to be satisfactory for radiation heating calculations.

The low frequency band systems of air are from the study by Biberman and Mnatsakanyan (Ref. 27). The high frequency band systems of air are also from Reference 27 for the band systems of NO and O₂; however, a combination of the data of Allen (Ref. 28) and that of Appleton and Steinberg (Ref. 29) is used for the N₂ contributions. The band systems for the ablation product species are from Arnold, Reis and Woodward (Ref. 30) for CN, C₂ and CO and from Weisner (Ref. 31) for C₂ and H₂.

4.2.4 Other Transitions

Several other transitions are known to be important under certain circumstances. The O₂ Shumann-Runge photodissociation continuum is approximated using the Sulzer-Wieland formula (see Ref. 32). The photodetachment cross-section for O⁻, H⁻ and C⁻ are from numerical data presented by Churchill et. al. (Ref. 33), Chandrasekhar and Elbert (Ref. 34) and Semon and Branscomb (Ref. 35), respectively. The importance of the N⁻ photodetachment contribution is currently being debated. When an N⁻ contribution is included in the present

model, the approach of Morris et. al. (Ref. 36) is utilized. The molecular photoionization cross-sections are from Biberman et. al. (Ref. 27) for NO and are not included for the other species. Finally, contributions due to particulate matter are not included due to a lack of reliable data. This limits the model to cases where particulate matter exerts only a negligible effect.

4.2.5 Numerical Evaluation of the Radiation Properties Model

The spectral contribution for each radiative transition for each species is considered individually. The continuum and line contributions are obtained from closed-form expressions when such are available. Otherwise, curve fits to numerical data are utilized.

4.3 TRANSPORT MODEL AND NUMERICAL SOLUTION PROCEDURE

4.3.1 Formulation

The basic equation governing the transfer of radiation through a medium in local thermodynamic equilibrium can be written as

$$\frac{dI_v}{ds} = \mu'_v (B_v - I_v) \quad (33)$$

where I_v is the spectral intensity, B_v is the Planck function, S is the length of the ray and μ'_v is the absorption coefficient corrected for induced emission, viz.

$$\mu'_v = \mu_v (1 - \exp(-h\nu/kT)) \quad (34)$$

where μ_v is the linear absorption coefficient.

In computing radiation fluxes across boundary and/or shock layers, the conventional plane parallel slab approximation is employed. Thus, the properties along any ray can be related to those along the normal coordinate (y) by applying a cosine transformation. The resulting expressions for the optical depth, spectral fluxes and total flux are well known and can be written in the form

$$\tau_v = \int_0^y \mu'_v dy \quad (35)$$

$$\left. \begin{aligned} F_v^+(y) &= \int_0^{\epsilon_b^+} E_v(\epsilon_v^+) d\epsilon_v^+ \\ -F_v^-(y) &= \int_0^{\epsilon_b^-} E_v(\epsilon_v^-) d\epsilon_v^- \end{aligned} \right\} \quad (36)$$

$$q_T(y) = \int_0^\infty [F_v^+(y) - F_v^-(y)] dv \quad (37)$$

where fluxes entering or reflected at $y = 0$ have been neglected (a cold, black wall is assumed). The quantity E_v is the black body emissive power defined as

$$E_v = \sigma B_v \quad (38)$$

and the emissivities ϵ_v^+ and ϵ_v^- utilized as independent variables in Equations (36) are defined by

$$\left. \begin{aligned} \epsilon_v^+ &= 1 - 2\mathcal{E}_3(t_v - \tau_v) \\ \epsilon_v^- &= 1 - 2\mathcal{E}_3(\tau_v - t_v) \end{aligned} \right\} \quad (39)$$

where the $\epsilon_n(x)$ functions are exponential integrals of order n .

The exponential approximation* is used to further simplify the equations without an appreciable loss in accuracy. Thus, the emissivities become

$$\left. \begin{aligned} \epsilon_v^+ &\approx 1 - \exp 2(\tau_v - t_v) \\ \epsilon_v^- &\approx 1 - \exp 2(t_v - \tau_v) \end{aligned} \right\} \quad (40)$$

*The second order exponential integral is approximated as $\mathcal{E}_2(x) = \exp(-2x)$ as suggested by Hunt and Sibulkin (Ref. 37). The usual recurrence relation then yields $\mathcal{E}_3(x)$.

which are more convenient to work with than those given by Equations (39). Emissivities written in this form have the additional advantage that by suppressing the factor of 2 in the exponential arguments and replacing E_ν by B_ν in Equations (36), the same formulation can be used to calculate intensities.

The transport integrals are considered to consist of two (line and continuum) parts. This allows optimum coordinates to be selected in frequency space. The continuum contribution to the absorption coefficient (μ_ν^C) is just the first term in Equation (27). Substituting μ_ν^C for μ_ν in Equations (35) and (36) yields corresponding values for τ_ν^C and F_ν^C , where the \pm signs have been dropped from the latter for brevity. The line contributions to the flux are obtained by difference

$$F_\nu^L \equiv F_\nu - F_\nu^C \quad (41)$$

where the F_ν values are evaluated using the total absorption coefficient (Eq. (27)). Thus, the line contribution is treated as a correction to the continuum flux.*

4.3.2 Numerical Evaluation of Flux Integrals

The transport integrals are now in a form suitable for numerical integration with no additional approximations required. The continuum fluxes, the approximation to the line fluxes for the high lines and high series, and the approximation to the molecular line fluxes can be calculated in a straightforward manner. The atomic and ionic line fluxes can be obtained exactly for the strong low-lying lines. While this latter calculation is lengthy, it is not felt to be excessively so. In all cases careful attention must be paid to the selection of nodal points (in frequency and in space) and interpolation formulas to insure that high accuracy is maintained.

For the continuum contribution to the flux integrals, the variation of both the Planck function and the continuum absorption coefficients must be adequately described. A priori selection of a frequency grid requires some care; fortunately it is only slightly dependent upon the characteristics of the layer. The first requirement can be met by distributing nodal points across the frequency range $h\nu \approx 0.25 \text{ eV}$ to $h\nu_{\text{max}} \approx 12 \text{ kT}_e \text{ eV}$ with about 30

* It should be noted that the line contribution defined by Equation (41) can be negative for nonisothermal layers.

points spaced at roughly equal intervals. This grid also satisfies the second requirement except in the ultraviolet where the frequency grid must be carefully selected to resolve the photoionization thresholds.

For the line contribution to the transport integrals, a frequency grid must be selected for each line and in general this should depend upon the characteristics of the layer as well as the individual line. This is accomplished by estimating in advance the distance in frequency space from the center of the line to the frequency corresponding to unity optical depth for a strong line or to the half intensity (or spectral flux) point for a weak line. This estimate is used to set the minimum frequency increment and the most remote nodal point for that particular line. A growth law is then used to establish smoothly varying frequency increments from the line center to the outermost point. Usually, 10 to 15 nodal points are sufficient to describe each line.

An initial spatial grid is selected so that it adequately describes the variations of the thermodynamic properties across the radiating layer. The optical depths are then calculated and used to evaluate the emissivities. When the layer is optically thin or of moderate optical depth, the initial grid can be retained; otherwise, a special grid is required. The layer is divided into equal increments of emissivities from which the new values of optical depth are calculated. The new E_ν values are then obtained by cubic interpolation in the plane $\ln E_\nu$ vs. $\ln \tau_\nu$. The new curve in the E_ν vs. ϵ_ν plane is suitable for accurate evaluation by numerical methods.

With one exception, all the integrals are evaluated using three term Taylor series expansions as interpolation formulas. The exception is the frequency integration of the continuum transport. Due to the discontinuities typically present in this integration, the series expansion is unsuitable and linear interpolation formulas are used.

4.4 THE RADIATION TRANSPORT PROGRAM (RAD)

4.4.1 Program Objectives

The RAD program generates the radiative properties model summarized in Section 4.2, and evaluates the corresponding transport integrals using the model summarized in Section 4.3. In both cases, the nongrey features of the models are retained. Radiative fluxes can be obtained directly, provided that the plane parallel slab approximation is invoked, or radiative intensities can

be obtained directly for any geometry. In either case, an arbitrary variation of thermodynamic state is allowed.

4.4.2 Program Input Requirements

The program requires a description of the spatial variation of temperature, pressure and mole fractions of the radiating species. It also requires a frequency grid for the continuum transport calculation and a set of frequency increments used to define the line groups. Finally, it requires an extensive set of basic spectroscopic data for the atomic and ionic species. This includes the energies and statistical weights of the electronic energy levels and the center frequencies, f-numbers and (half) half-widths of the lines.

4.4.3 Program Capabilities

The program has the following special features which can be utilized when it is operating in either the flux calculation or the intensity calculation mode:

- a. A frequency dependent transmissivity can be assigned to any spatial station. This allows the program to simulate laboratory experiments in which the incident radiation is observed through a window.
- b. A switch is available which can be used to include or remove any of the continuum contributions to the properties model. This allows the relative importance of the different radiation species to be assessed.
- c. The properties of the lines within a given line group can be combined to form an "average" line, or each line can be considered individually. This allows trade-offs to be made between accuracy and computational efficiency.
- d. A special input option is available for cases where the thermodynamic properties do not vary spatially. It greatly reduces the labor required to prepare the input data.

Under normal operating conditions the program calculates and can be instructed to print out the following quantities: spectral absorption coefficients and optical depths, continuum contributions to the spectral and total fluxes (or intensities), spectral (line + continuum) fluxes (or intensities) and the contributions due to atomic and ionic lines.

4.4.4 Program Storage Requirements and Computational Time

The program requires roughly 15,500 words of core storage on the Univac 1108. On machines such as the Philco 212 or the CDC 6400 where more than one instruction can be stored in a word, the core requirements are noticeably less.

The computational time depends on the number of spectral lines considered and the number of spatial stations at which the transport integrals are to be evaluated. Typically it takes approximately 30 seconds of Univac 1108 time to calculate the flux at one spatial station for an air plasma with about 85 lines considered individually. The extrapolation of the calculational time to greater numbers of lines and/or spatial nodes is not linear - each succeeding calculation taking less time than the initial one. Typical calculation times are about ten to fifteen seconds per node for a boundary layer calculation considering C-H-O-N elemental system (seven nodal points considered).

4.4.5 Program Utilization

The code, although recently developed, has already received rather extensive utilization. A variety of cases are reported in Part III. In addition, a calculation of the flux transmitted across an Apollo-type boundary layer is reported in Section 6.5.

4.5 CONCLUDING REMARKS

The model described can be used to obtain fluxes or intensities at any specified point within a plane-parallel slab (for the flux calculation) or at any point on a ray of interest (for the intensity calculation). The model was developed specifically for the study of radiation heating phenomena within the boundary layer over an ablating surface. Therefore, it is most detailed in those ranges of temperature and pressure where the radiative energy flux should be equal to or greater than the diffusive energy flux. Highly detailed spectral resolution was maintained only when it was required to obtain accurate total fluxes (or intensities).

SECTION 5

ANALYSIS AND COMPUTATIONAL PROCEDURE FOR RADIATION COUPLED BOUNDARY LAYERS (RABLE PROGRAM)

An approach for analyzing radiation coupled hypersonic boundary layers has been developed by incorporating a subroutine version of the RAD program into the BLIMP nonsimilar laminar boundary layer procedure. The approach is formulated in Section 5.1, while the computational procedure is outlined in Section 5.2. The resulting program, termed the Radiating Boundary Layer Environment (RABLE) code, is described in Section 5.3.

5.1 FORMULATION

The radiation coupled boundary layer problem has been formulated in terms of the nonsimilar laminar boundary layer equations discussed in Reference 3 extended to allow a radiation contribution to the flux term in the energy equation. The nongrey radiative transport model discussed in Part III of this series of reports and summarized in Section 4 is used to calculate this contribution. The boundary conditions on the boundary layer equations are unchanged.* In addition, split boundary conditions are employed for the radiation flux calculation with the inward directed flux being specified at the boundary layer edge and the outward directed flux specified at the wall (taken to have a negligible interaction with the gases of the boundary layer in comparison with the interactions of the other fluxes present there). For each boundary condition, the flux in the opposite direction and, consequently, the net flux is obtained from the calculation.

The resulting formulation has all the capabilities and limitations of its components. For example, this includes multicomponent diffusion and equilibrium chemistry for general chemical systems; a variety of coupled and uncoupled surface boundary conditions; nongrey emission and absorption by the continuum, molecular bands, and atomic lines of the radiating species of the C-H-O-N elemental system; and nongrey transport of radiant energy using the tangent slab approximation.

*Thus, the adiabatic edge condition is retained. This is consistent with the boundary layer approach to this complex problem and is valid as long as the edge of the thermal boundary layer is not so far from the wall as to invalidate the boundary layer approximations.

5.2 SOLUTION PROCEDURE

A successive approximation iteration scheme is presently used to obtain radiation coupled solutions. Initially, a solution to the boundary layer equations is obtained in the usual manner (see Section 2.1) which does not include a radiation contribution. The spatial distribution of the radiation flux is calculated from the transport integrals and introduced directly into the energy error equation of the integral matrix procedure. The Newton-Raphson iteration then drives the errors of the boundary layer equations to zero (while holding the radiation fluxes unchanged*) to obtain new distributions for the thermodynamic state and flow field quantities. A new radiation flux distribution is obtained by evaluating the transport integrals and averaging the results with the previous flux distribution. This damps the oscillations which would otherwise be introduced by this out-of-phase calculation. The iteration cycle is completed by replacing the previous flux distribution with the newly obtained one. This procedure is repeated, iterating on the radiation flux distribution, until convergence is obtained.

The primary advantage of the successive approximation iteration scheme is its simplicity, viz. the derivatives of the radiative flux term with respect to the primary variables are not required. It is an effective iteration scheme provided that the radiation fluxes are not dominant. Under this condition, solutions are obtained easily with only a few (3 or 4) iterations being required. However, the iteration scheme cannot be expected to be efficient for radiation-dominated problems.

5.3 THE RABLE PROGRAM

A subroutine version of the RAD program has been incorporated into the BLIMP program to form the RABLE program. The coupling of these two programs was particularly straightforward since they were both developed with this ultimate intention. The primary modifications of the BLIMP program were (1) the insertion of a call of RAD to compute the net radiation heat flux at each boundary layer nodal point, (2) the addition of this heat flux term into the energy error equation in the Newton-Raphson iteration, and (3) the development of the convergence acceleration scheme to allow converged boundary layer

*The procedure of utilizing only converged boundary layer solutions for the radiation flux calculation (rather than the usual procedure of calculating the flux after each iteration) tends to increase the number of boundary layer iterations while decreasing the number of radiation calculations. This approach was motivated by economic considerations, each radiation calculation requiring about 35 times as much effort as a boundary layer iteration.

solutions to be obtained in between each call of the RAD program. Modifications to the RAD code included a new subroutine to generate the external boundary flux, a new subroutine to identify the BLIMP variables in terms of the RAD variables, and the flux averaging scheme used to damp the iterations.

A calculation of an Apollo type superorbital entry condition has been performed and is presented in Section 6.6. Three radiation iterations were required for the calculation to converge. The total computation time was about 6 minutes on the Univac 1108.

SECTION 6

APPLICATION OF CODES TO APOLLO HEAT SHIELD PROBLEMS

6.1 INTRODUCTION

The computer codes described in the previous sections can be used to predict convective and radiative heating rates, ablation rates, and internal thermal response for arbitrary materials, environmental gases, and flight conditions, taking into account radiation-convection coupling and coupling between the boundary layer and material response. In this section the use of the codes is illustrated by applying them to problems associated with the Apollo heat shield during superorbital earth reentry.

A CMA Option 2 calculation (assigned surface temperature and char recession rate) is compared in Section 6.2 to thermocouple data from a recent superorbital Apollo flight. Normalized ablation rates obtained with the ACE program are presented in Section 6.3 and compared to BLIMP solutions for the same surface models. In Section 6.4, BLIMP predictions are presented for the boundary layer along the windward ray of the Apollo vehicle during a recent simulated lunar return trajectory and for the stagnation point during 50,000 feet per second reentry, both considering wall steady-state energy balances. In Section 6.5, a RAD solution is presented which demonstrates radiative flux distributions in a boundary layer contaminated by ablation products for an Apollo flight condition near peak heating. In Section 6.6, RABLE is employed to generate a radiation-coupled boundary-layer solution for the same flight condition considered in the RAD solution of Section 6.5. Coupled transient predictions for Apollo material response obtained with the CMA/ACE and CABLE programs are presented in Sections 6.7 and 6.8, respectively. These solutions also correspond to a recent superorbital Apollo flight.

6.2 DRIVER TEMPERATURE CALCULATIONS USING CMA OPTION 2

The CMA program, Option 2, is useful to assess the validity of a material thermal properties model. Since surface temperature and surface recession histories are not usually very accurately known, it is appropriate to consider the response of a thermocouple located near the surface as a "driver temperature" and to compare the response of thermocouples located further into the material to predicted temperatures at these thermocouple locations. With this technique, the surface recession rate is zero throughout the test. A study of a thermal properties model for the Apollo heat shield material using this approach is presented in Part II of this series of reports. Both ground data

and data from a recent superorbital flight are considered therein. One of the correlations of flight data from this study is presented in Figure 1. In this particular calculation, a thermocouple originally 0.30 inches from the surface has been used as the driver.

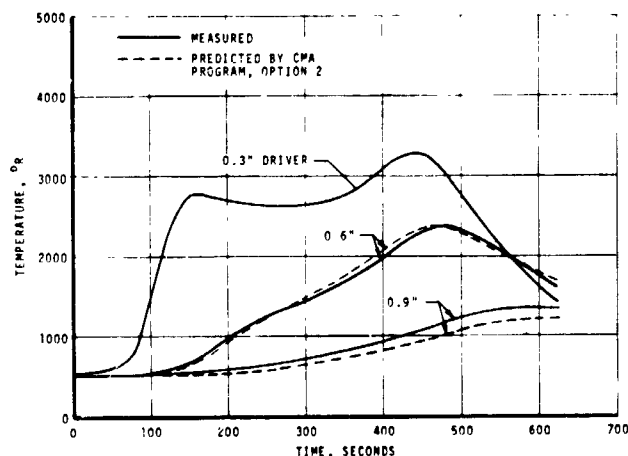


Figure 1. Correlation of In-Depth Temperature Response of Apollo Flight Data Using 0.3-Inch Thermocouple as a Driver

6.3 NORMALIZED ABLATION TABLES GENERATED BY ACE PROGRAM

One of the principal uses of the ACE program is to generate tables of char recession rate normalized by mass-transfer coefficient, B'_C , versus surface temperature for various values of normalized pyrolysis gas rate, B'_g , and pressure. The ACE program does not provide the transfer coefficients (and thus the \dot{S}) nor does it perform a surface energy balance (needed to provide T_w). Rather, the output from the ACE program is used as input to the CMA program together with convective transfer coefficients. The CMA program then provides an energy balance to obtain coupled transient solutions.

In Part II of this series of reports, a comprehensive study of ground and flight test data using the ACE program as a primary tool is reported. A number of parameters were varied in an attempt to achieve consistent correlation of the data. Some of the parameters which were considered were pyrolysis gas reactivity with the boundary-layer gases, changes in surface elemental composition due to in-depth coking reactions, mechanical removal of candidate surface species, loss of pyrolysis gas through fissures which are seen experimentally to develop in the chars, and surface thermochemistry including silica-

carbon reactions. It is shown therein that thermochemical ablation theory (without mechanical removal mechanisms) is satisfactory only at relatively high surface temperatures and then only if it is assumed that the pyrolysis gases are not effective in blocking the convective heat transfer (so-called fissure model). At lower surface temperatures, it is necessary to employ a rate law for the mechanical removal of silica in the char material. ACE solutions based on this model are compared in Figure 2 to the ground test data of Schaefer et. al. (Ref. 38).

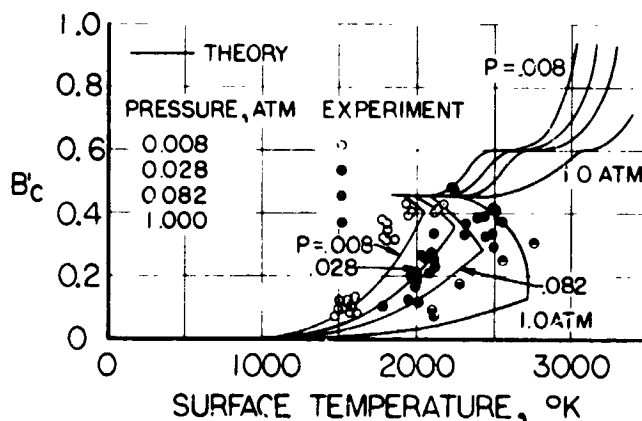


Figure 2. Comparison with Ground Test Data of Noncoking Fissure Surface Thermochemistry Model Including $B'_c \sqrt{P}$ Correlation for Mechanical Removal of Silica

It is also demonstrated in Part II of this series of reports that the ACE and BLIMP programs produce identical results for B'_c versus T_w , but that the BLIMP program provides, in addition, the mass-transfer coefficient (and thus \dot{m}_w) and, when the steady-state energy balance option is employed, also provides the resulting T_w . Thus, relative to BLIMP, ACE is not an approximate theory, but a partial theory. It becomes approximate in application only when mass-transfer coefficients are assumed in order to achieve an answer. ACE solutions for a nonfissure, inert-pyrolysis-gas model for a steady-state ratio of B'_g to B'_c are compared in Figure 3 to some BLIMP solutions. Solutions are shown both considering a $\dot{S} - T_w$ rate law for mechanical removal of silica developed from the results of Figure 2 and neglecting this rate law (in which case the onset of ablation is delayed to much higher temperatures where the silica is hot enough to vaporize). It can be seen that the agreement between the BLIMP and ACE solutions is indeed precise.

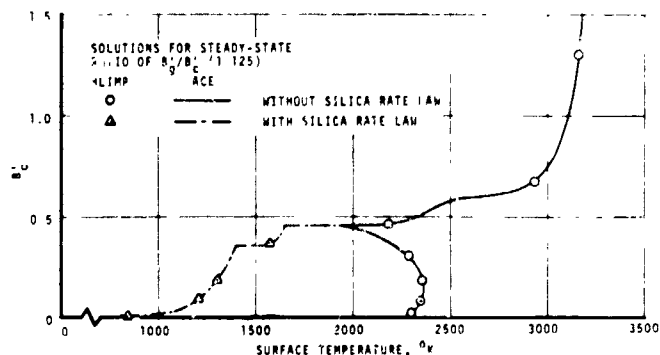


Figure 3. Comparison of Surface Thermochemistry Maps for Nonfissure Model with Rate Law for Mechanical Removal of Silica as Generated by BLIMP and ACE Programs ($H_T = 25,000$ Btu/lb, $P_{T_2} = 0.028$ atm)

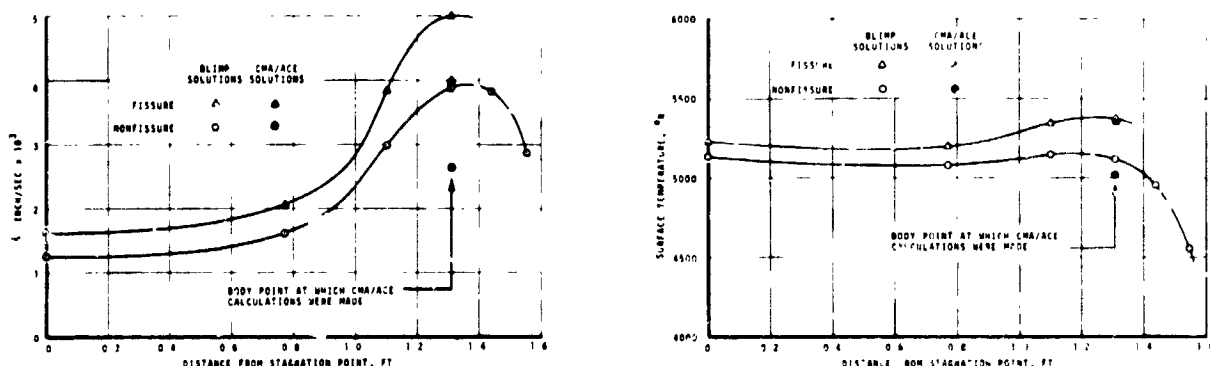
6.4 STEADY-STATE ABLATION PREDICTIONS USING BLIMP

The BLIMP program has many uses in the study of a flight vehicle such as Apollo. For example, it can be used in its uncoupled modes to predict convective heating rate distributions including nonsimilar effects, to predict blowing reduction parameters and effective heats of combustion for use with simplified analyses, and to generate detailed profiles throughout the boundary layer for communication studies. However, it can also be used to predict steady-state ablation rates and surface temperatures while considering the detailed structure of the boundary layer. In the steady-state asymptote, the requisite parameters (conduction into the body and the ratio of \dot{m}_g to \dot{m}_c) are known without further consideration of in-depth response. The results of steady-state ablation solutions for a recent superorbital flight and for a 50,000 fps trajectory are presented in the following subsections. The prediction of transient ablation rates while considering the detailed structure of the boundary layer requires use of the CABLE program which couples BLIMP to CMA. A CABLE solution is presented in Section 6.8.

6.4.1 Solutions for a Recent Superorbital Apollo Flight

In Part II of this series of reports, BLIMP solutions are presented for steady-state ablation along the windward ray of the Apollo vehicle for flight conditions corresponding to peak heating in a recent superorbital Apollo flight. In these calculations, the incident radiation fluxes were assigned at values provided by NASA MSC and were considered unattenuated in the boundary layer. Two models for surface thermochemical ablation were considered, a model where the pyrolysis gas was considered inert but allowed otherwise to interact with the boundary layer (nonfissure model) and a model where the

pyrolysis gases were considered to escape through the boundary layer without altering boundary layer profiles (fissure model). Distributions of surface recession rate, \dot{S} , and surface temperature, T_w , generated in this study are presented in Figure 4. Transient solutions obtained with the CMA/ACE approach at a body station 1.31 feet downstream of the stagnation point are shown for comparison. It can be seen that the CMA/ACE predictions for surface temperature were excellent, whereas the BLIMP program predicted \dot{S} approximately 30 percent higher. The primary reason for this discrepancy is that the nonablating heat-transfer coefficients predicted by BLIMP at this station are about 40 percent higher than the values supplied by NASA MSC which were used as input in the CMA/ACE calculations.



(a) Surface Recession Rate

(b) Surface Temperature

Figure 4. Boundary Layer Solutions Along Apollo Windward Ray for Fissure and Nonfissure Models Considering Steady-State Surface Energy Balances for Typical Super-orbital Trajectory (Time = 30,030 sec)

6.4.2 Solutions for a 50,000 Feet-Per-Second Trajectory

A set of steady-state calculations utilizing the BLIMP program was also carried out in which the Apollo heat shield material was subjected to a hypothetical trajectory, provided by NASA MSC, with an entry velocity of 50,000 ft/sec and an entry angle of -7.65 degrees. This trajectory results in a single peak in heating rather than the double peaked curve which is more typical of lunar return Apollo flights. The trajectory information as supplied by NASA MSC is shown in Table II. Of particular interest is the fact that the peak radiative heating rate is $,800 \text{ Btu/ft}^2\text{sec}$, an order of magnitude larger than the convective heating rate and an order of magnitude larger than the maximum total heating rate for conventional Apollo trajectories.

TABLE II
NASA 50,000 FPS TRAJECTORY

Time Sec.	q_{conv} Btu/ft ² sec	q_{rad} Btu/ft ² sec.	Velocity ft/sec	Altitude Ft.
0	4.93	0.	48461.	400000.
10	19.76	0.	48500	337700.
20	88.88	40.	48522.	283900.
30	275.06	780.	48348.	239100.
40	500.00	3600.	47300.	207000.
45	560.86	5100.	46238.	195300.
49	556.79	5800.	45170.	190000.
55	531.38	5500.	43231.	186800.
60	506.00	5030.	42000.	186800.
70	400.00	3350.	39300.	
80	317.	1720.	37100.	
90	265.	1000.	35000.	
100	227.	530.	33200.	
110	200.	200.	31700.	
115	186.40	100.	31000.	
120	175.	30.	30000.	
130	153.	26.	28700.	
140	135.	22.	27500.	
150	118.	18.	26400.	
160	105.	14.	25500.	
170	93.	10.	24500.	
180	81.	8.	23700.	
190	72.	6.	22700.	
200	66.	5.	22200.	
220	55.	4.	21500.	
240	45.	3.	19600.	
260	38.	2.	18500.	
300	26.	1.	16600.	186800.
350	18.	.5	14700	185000.
400	14.	0.	13100.	177000.
450	11.	0.	11200.	164000.
500	7.	0.	8800.	144000.
550	4.	0.	6000.	131000.

In these calculations, the pyrolysis gas was considered to be inert but to otherwise interact with the boundary layer (nonfissure model). The surface was considered to be in equilibrium with the gases adjacent to the surface and a steady-state energy balance was performed at the wall. As in the calculations of Section 6.4.1, the incident radiation was considered to be unattenuated in the boundary layer and to enter directly into the surface energy balance.

The convective heat flux to the wall computed by BLIMP is presented in Figure 5 together with the radiative and nonablating-convective heat fluxes supplied by NASA MSC. It can be seen that the convective heat flux is essentially reduced to zero from 30 to 80 seconds in the trajectory indicating the boundary layer has blown off the surface. This is illustrated even more dramatically in Figure 6 which shows temperature distributions between 25 and 49 seconds. At the most severe condition of 49 seconds, it can be seen that the thermal boundary layer is blown about 8 inches off the surface.

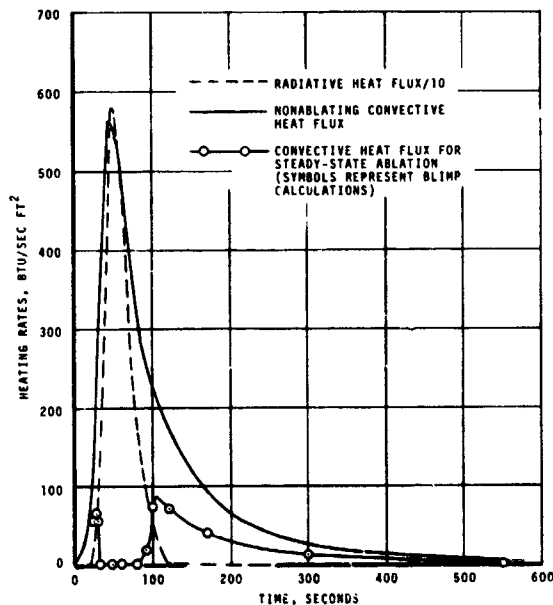


Figure 5. Convective and Radiative Heating Rates to Stagnation Point of Apollo Vehicle During Typical 50,000 fps Reentry

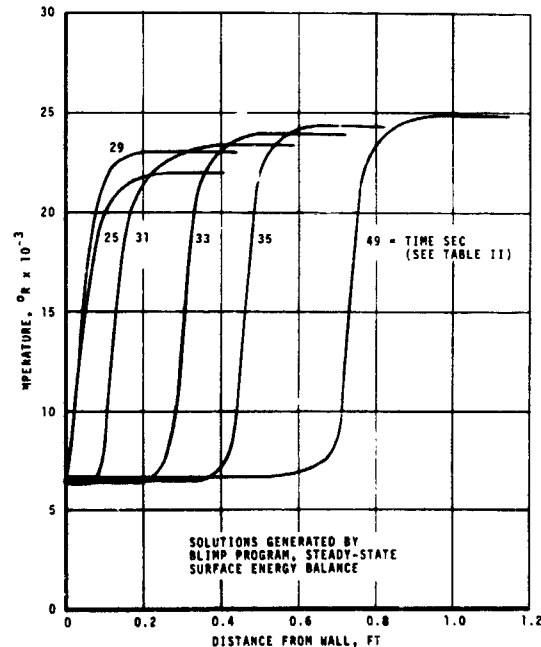


Figure 6. Temperature Distributions Across Apollo Stagnation Point Boundary Layer During Typical 50,000 fps Reentry

In order to demonstrate further the nature of the calculations which were performed, mole fraction distributions across the boundary layer are presented in Figure 7 for a trajectory time of 31 seconds. It can be seen that even at this relatively early time the composition of the gas at the wall represents over 99 percent ablation material. It should be recalled that the mass balance and equilibrium calculations at each point in the boundary layer are performed during the course of the boundary layer calculation and are fully coupled with energy and momentum considerations.

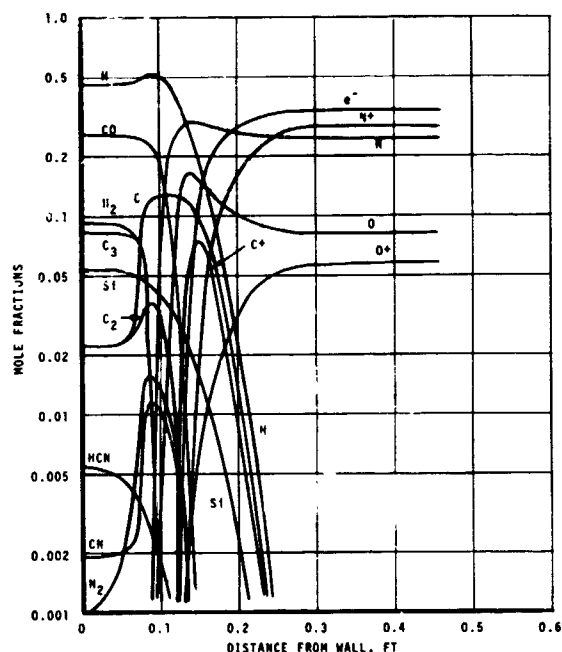


Figure 7. Mole Fractions Across Apollo Stagnation Point Boundary Layer During Typical 50,000 fps Reentry (Time = 31 sec)

Surface temperature, surface recession rate, and integrated surface recession are presented as functions of time in Figures 8, 9 and 10, respectively. The predicted surface temperature attains a maximum of 6,750°R. There is some question whether the rather fragile char would survive at such high temperatures. The peak surface recession rate is predicted to be 0.14 inch/sec, while the total surface recession, most of which occurs over a 45-second period of time, is 4.64 inches. These values could be higher if the char cannot structurally survive the very high surface temperatures which are predicted. On the other hand, the incident radiation may be appreciably blocked

by the ablation products in which case less ablation would be predicted. Finally, a correlation of surface recession rate versus radiative heat flux is presented in Figure 11. It can be seen that for radiative heat fluxes, q_r , above 1,200 Btu/sec-ft² or so, the surface recession rate is predicted quite accurately by the simple linear relation

$$\dot{S} = 3.04 \times 10^{-5} (q_r - 960) \quad (42)$$

with \dot{S} in inches/sec and q_r in Btu/sec-ft². Such a linear asymptotic relation would be expected from the heat-of-ablation concept.

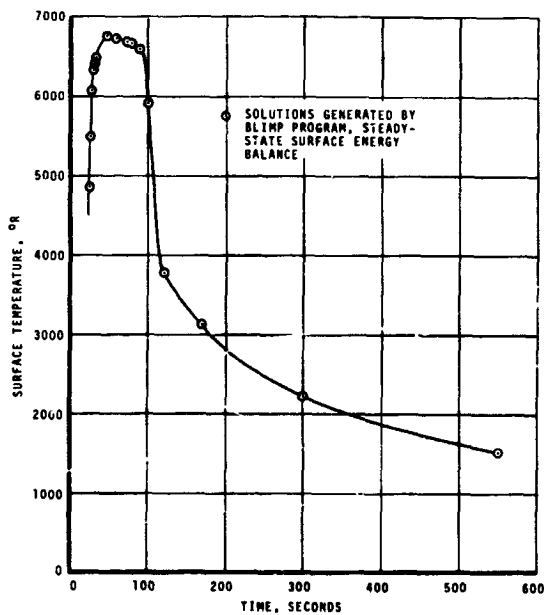


Figure 8. Surface Temperature History for Apollo Stagnation Point During Typical 50,000 fps Reentry

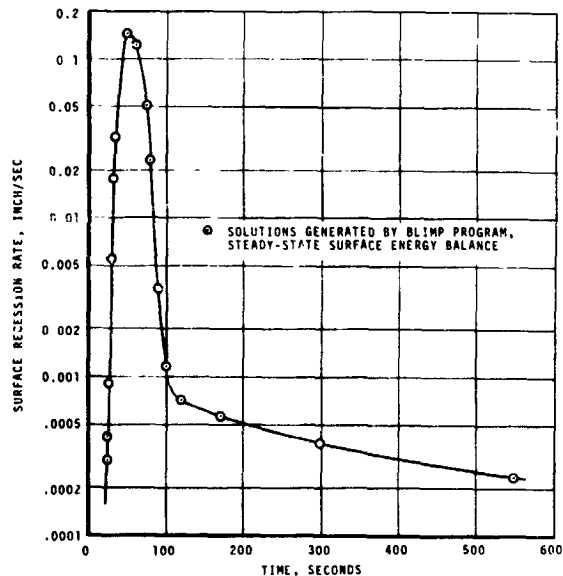


Figure 9. Surface Recession Rate History for Apollo Stagnation Point During Typical 50,000 fps Reentry

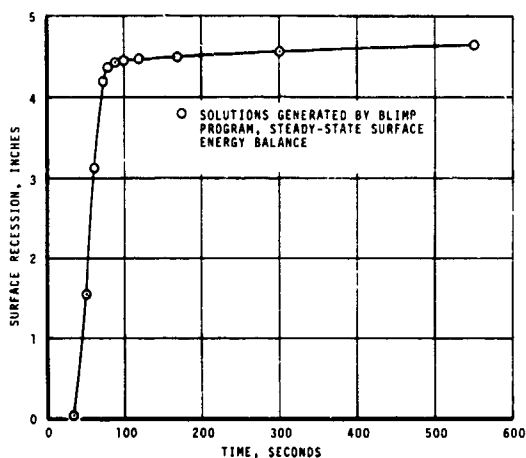


Figure 10. Surface Recession History for Apollo Stagnation Point During Typical 50,000 fps Reentry

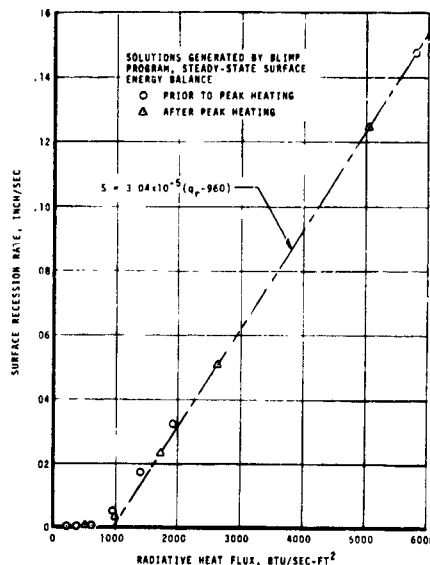


Figure 11. Correlation of Surface Recession Rate Versus Radiative Heat Flux for Apollo Stagnation Point During Typical 50,000 fps Reentry

6.5 UNCOUPLED CALCULATION OF RADIATIVE FLUX DISTRIBUTION USING THE RAD PROGRAM

A number of calculations have been performed with the RAD program to obtain distributions of radiative flux or intensity across layers of varying thermodynamic state. One such calculation - the flux distribution across a highly blown, hypersonic boundary layer - is presented here to illustrate the kind of information which can be obtained from the program. Additional calculations are given in Part III of this series of reports.

The spatial distributions of pressure, temperature and mole fractions are from a radiation coupled boundary layer solution (RAPLE program) and are characteristic of the conditions found on the front face of the Apollo vehicle just after the maximum heating point on its trajectory. The distributions* for the temperature and mole fractions of the radiating species are shown in Figures 12 and 13 (the dashed curves). The pressure was taken to be 0.467 atmospheres and assumed to be constant across the layer. An incident flux of 53 Btu/ft²-sec was specified on the outer edge of the boundary layer, and

*The Levy-Lees variable η has been used in presenting the data. The following list can be used to convert these to spatial points:

$$\eta = 0, 1.07, 2.497, 4.458, 7.133, 10.70, 17.83$$

$$y(\text{ft}) = 0, 4.45 \times 10^{-3}, 0.01055, 0.01988, 0.04048, 0.0812, 0.1728$$

one of zero Btu/ft²sec at the wall (cold, black wall assumption). The radiative flux distributions were actually calculated using the RAD subroutine to the RABLE program but are the same as those which would have been obtained with the uncoupled program using the same input quantities. The tangent slab approximation was employed for all cases.

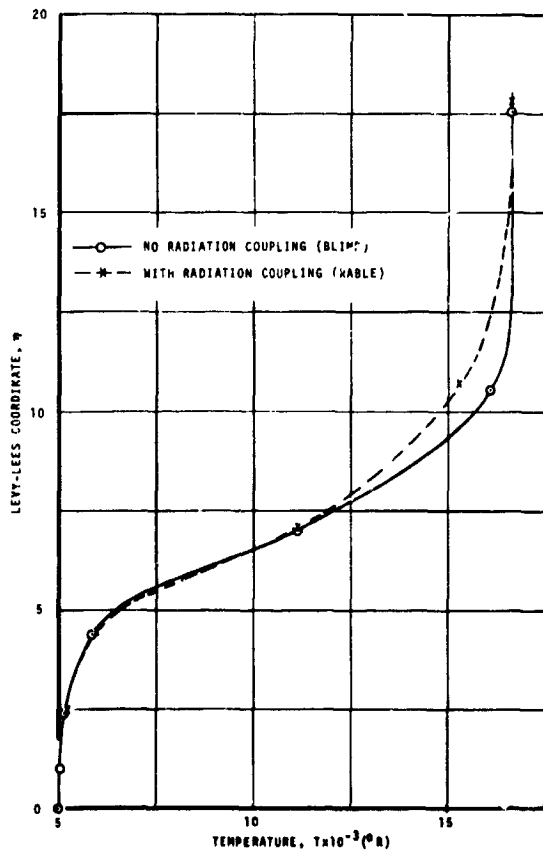


Figure 12. Effect of the Radiative Coupling on the Temperature Distribution for Typical Apollo Superorbital Trajectory (Time = 30,045 sec)

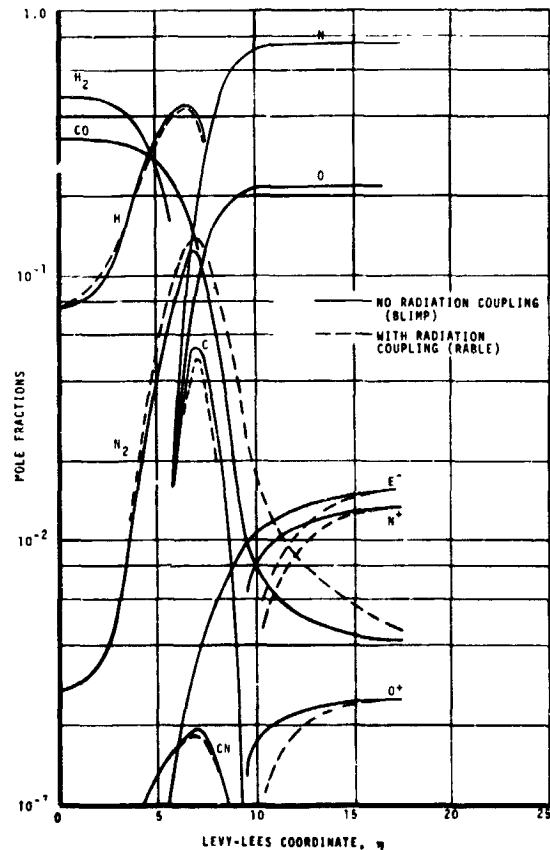


Figure 13. Effect of Coupling on the Spatial Distribution of the Radiating Species for Typical Apollo Superorbital Trajectory (Time = 30,045 sec)

The distributions taken from the boundary layer calculation show that three fairly distinct regions exist. The inner region $\eta < 5$ or so is primarily composed of the molecular products of ablation. The ablation model which yielded this particular distribution will be discussed in Section 6.6. Further out ($5 < \eta < 9$), a mixing region exists where both the elemental composition and the temperature of the layer are changing rapidly. The CN

molecule, which can be expected to radiate strongly, appears only in this region and only in low concentrations. The outer region ($\eta > 9$) is composed of slightly ionized air and experiences only a very mild temperature gradient.

The spatial distributions of the positive (inward directed) and negative (outward directed) fluxes (F^+ and F^-) are shown in Figure 14. The positive flux starts with its assigned contribution at the outer boundary and remains nearly unchanged as it passes through the outer region. As it enters the mixing region, it increases noticeably in spite of the fact that the temperature is dropping sharply. It then tails off through the inner region to the wall value. The negative flux starts at its assigned value (zero) at the wall and remains unchanged through the cool inner region. It then increases sharply through the mixing region and the outer region, feeling the effects of more efficiently radiating species and increasing temperature.

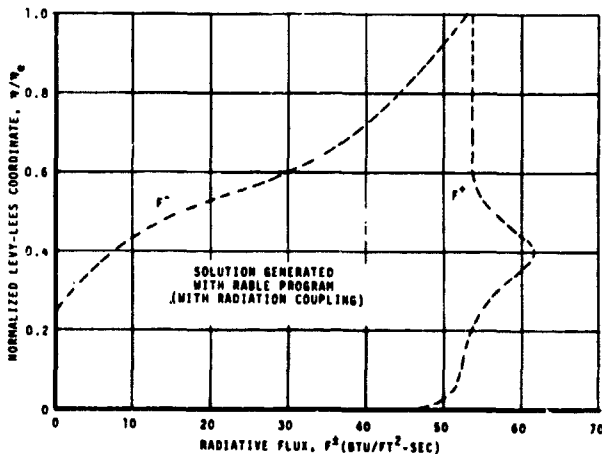


Figure 14. Spatial Distributions of the Radiative Fluxes in the Positive and Negative Directions for Typical Apollo Superorbital Trajectory (Time = 30,045 sec)

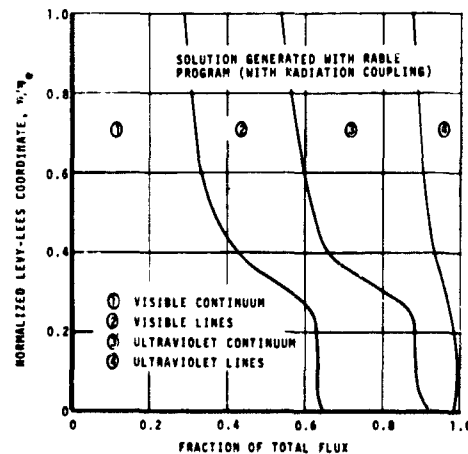


Figure 15. Components of the Radiative Flux Directed Toward the Wall for Typical Apollo Superorbital Trajectory (Time = 30,045 sec)

Figures 15 and 16 help to clarify the physical events which are occurring. The positive flux undergoes a major change in its spectral distribution as it crosses the mixing layer. Its energy is distributed in a 2-to-1 ratio (see Figure 15) between the visible and ultraviolet frequencies as it enters, a 9 to 1 ratio as it leaves. The spectral distributions of the continuum

contribution of F_{ν}^+ given in Figure 16 indicate that a great deal of the ultra-violet part of the boundary flux is absorbed; while a (roughly) equal amount is emitted by the CN bands in the visible. Thus, the modest variation of the positive flux as it passes through the mixing layer is the result of a competition between these two strong effects. In the case of the negative flux, the two effects combine rather than compete to cause the dramatic increases in the flux levels. The final tail-off of the positive flux in the inner region can be attributed to the absorption of a small emission peak in the near-ultraviolet, apparently due to the H_2 Lyman band system. The positive flux at $\eta = 2.40$ (and for $5\text{ev} < h\nu < 8\text{ev}$) is also shown in Figure 16 where this peak is in evidence.

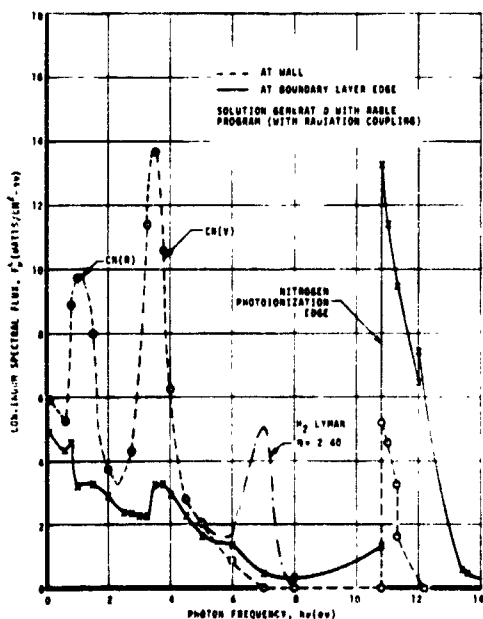


Figure 16. Spectral Distribution of the Continuum Flux Directed Toward the Wall for Typical Apollo Superorbital Trajectory (Time = 30,045 sec)

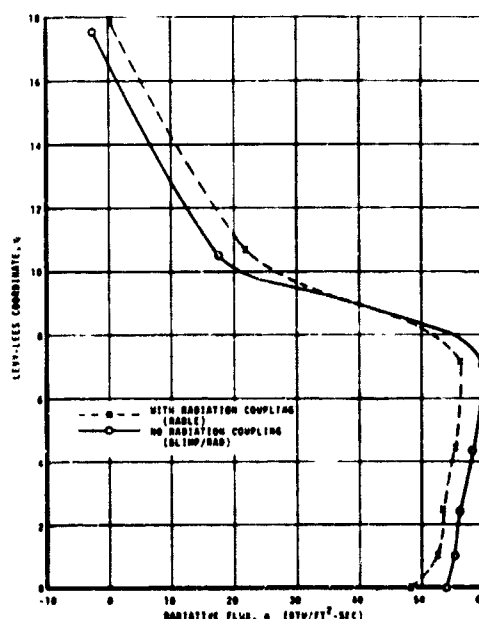


Figure 17. Effect of Radiative Coupling on the Net Radiative Flux Distribution for Typical Apollo Superorbital Trajectory (Time = 30,045 sec)

The distribution of the net radiation flux is shown in Figure 17. The distribution in the inner region is essentially that of the positive flux. The distributions in the mixing and outer regions are dominated by the behavior of the negative flux. Judging from the slope of the curve, it appears that the radiation losses toward the bow shock become greater than those toward the wall at a point just outside the edge of the boundary layer.

6.6 A CALCULATION OF THE RADIATION COUPLED BOUNDARY LAYER USING THE RABLE PROGRAM

A RABLE program solution is presented here to illustrate both the kind of information which can be obtained from the program and the type of effects which occur. The solution is for the stagnation point conditions at the maximum ablation point of a recent Apollo superorbital trajectory and the same as the one used in Section 6.5. Edge conditions are $H_T = 19,282$ Btu/lb and $P = 0.476$ atm. The blowing rates are taken to be 1.37×10^{-2} lb/sec-ft² for the pyrolysis gas and 7.611×10^{-3} lb/sec-ft² for the char removal rate. The elemental composition of the pyrolysis gas is consistent with a coking ablation model in which the pyrolysis gas is in equilibrium with the char layer (see Part II of this series of reports).

The distributions across the boundary layer are shown with and without radiation coupling in Figures 12, 13 and 17. The temperatures tend to cool in the mixing and outer regions of the layer. This corresponds to rapid changes in the net radiative flux as shown in Figure 17 and attributed previously (Section 6.5) to sharp changes in the negative flux due to CN and N photoionization contributions. The inner region experiences only a very slight interaction with the radiative flux. This occurs because the incident flux which can be absorbed there (the ultraviolet) is trapped in the mixing layer and cannot get through to either the inner region or the wall.

The coupling effects on the distributions of the mole fractions of the radiative species are shown in Figure 13. The degree of ionization is changed appreciably as is the fraction of undissociated N_2 . It would appear that the Saha equilibrium condition which governs these concentrations is in a range which is very sensitive to small temperature changes. The species which are present in large concentrations undergo only insignificant changes.

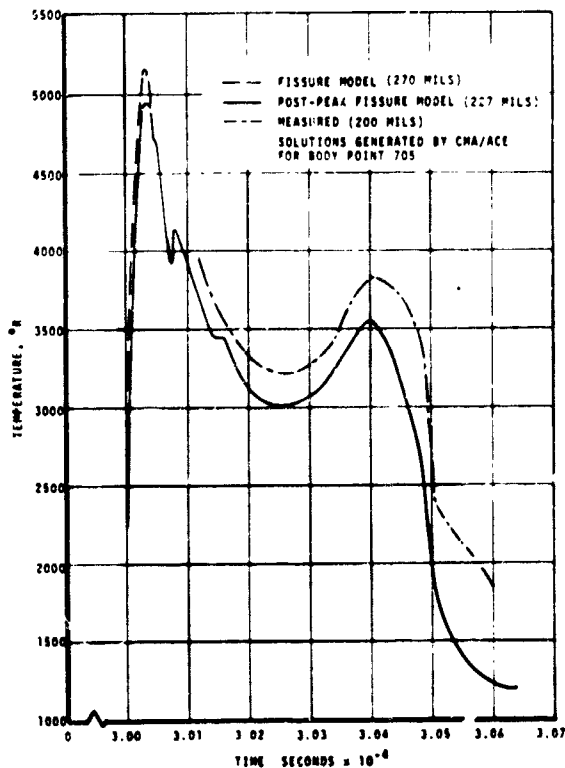
The distributions of the net radiative flux given in Figure 17 indicate that the coupled net flux is smaller in the inner region and larger in the outer region. This can be attributed to a decrease in emission in the mixing layer due to the lower temperatures. Thus, a smaller amount of energy is added to the positive flux (causing the net flux in the inner region to be less), and a smaller amount of energy is added to the negative flux causing the difference between the positive and the negative fluxes (the net flux) to be greater in the outer region. The net radiative flux at the wall is decreased by 15.5 percent due to this coupling. The diffusive flux at the

wall is not significantly changed in the present problem since in either case it is very small (about 1 percent of the radiative flux).

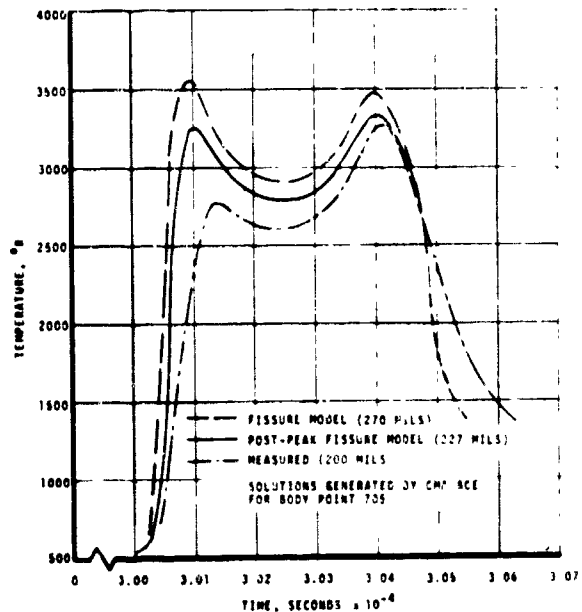
6.7 COUPLED TRANSIENT SOLUTIONS USING CMA/ACE APPROACH

Once a set of ACE solutions of the type discussed in Section 6.3 are generated, the resulting punched card output can be used as input to the CMA program to obtain coupled transient ablation predictions. A number of such solutions for a recent superorbital Apollo flight are presented in Part II of the present series of reports considering various assumed surface physicochemical models. In order to demonstrate the nature of the solutions, results for two of these models are presented in this section. The first model considers fissures (where the pyrolysis gases are not effective in blocking the convective heating) throughout the flight, whereas the second considers fissures only after peak heating.

Surface temperature and temperatures 0.3 and 0.9 inch from the original surface are compared to measured temperatures in Figure 18(a) through (c),

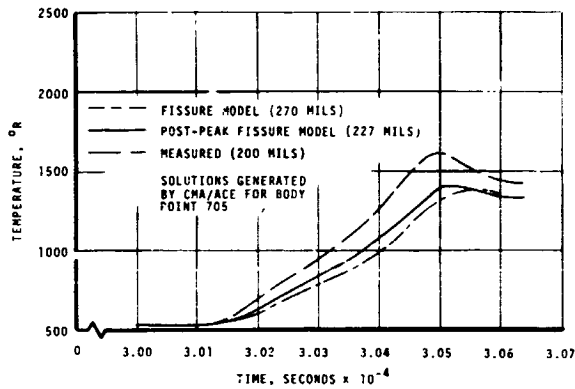


(a) Surface Temperature



(b) 0.3 Inch from Initial Surface

Figure 18. Temperature Histories for Typical Superorbital Trajectory with Fissure and Post-Peak Fissure Models



(c) 0.9 Inch from Initial Surface
Figure 18. Concluded

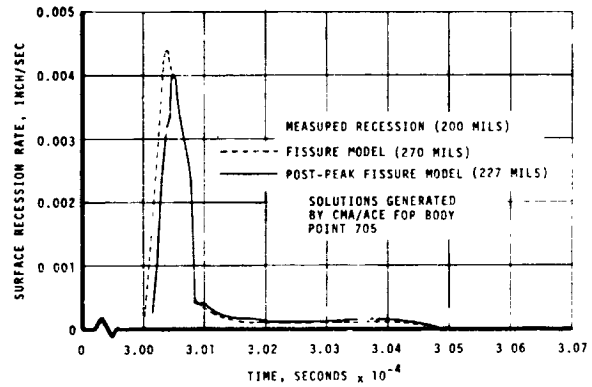


Figure 19. Surface Recession Rate
Histories for Typical
Superorbital Trajectory
with Fissure and Post-
Peak Fissure Models

respectively. Agreement with flight temperatures is considered quite good, especially for the post-peak fissure model where reduction of convective heating rates by the pyrolysis gases prior to peak heating decreases the in-depth temperatures throughout the entire flight. Surface recession predictions, shown in Figure 19, are in substantial agreement with the measured total recession for the body point and flight considered for both fissure and post-peak fissure models. (Various nonfissure models which were considered in Part II substantially underpredicted the surface recession.)

6.8 COUPLED TRANSIENT SOLUTION USING CABLE PROGRAM

As a demonstration of the CABLE program, a coupled transient solution at the stagnation point of the Apollo heat shield during the first 80 seconds of a recent Apollo superorbital flight is presented in this section. An inert pyrolysis gas nonfissure model with a silica fail temperature of 1,620°R was considered in this calculation.

As discussed in Section 2.5, the CABLE program operates, in effect, with CMA as the controlling program, calling the BLIMP routine as needed to supply information for the ablating-wall surface boundary condition. In the present calculation, the BLIMP program was called 88 times. This sequence of BLIMP solutions is discussed in detail in Appendix A, together with a discussion of solutions obtained at the second streamwise station.

Temperature distributions at the stagnation point through the charring ablation material and boundary layer, running all the way from the back wall to the boundary-layer edge, are presented in Table III for the six times considered. Pyrolysis gas and char recession rates are also summarized in Table III.

Elemental mass fractions across the boundary layer at 30,020 seconds are presented in Figure 20 in order to demonstrate the severity of some of these boundary layer solutions. In this figure the inert pyrolysis gas is identified as PYROL. It contains carbon, oxygen, hydrogen and nitrogen in accordance with what is considered to be the products of the primary pyrolysis. It can be seen that over 99 percent of the gas at the wall is PYROL, most of the remaining gas being the char products of carbon, silicon and oxygen. The amount of nitrogen that is able to diffuse to the wall from the

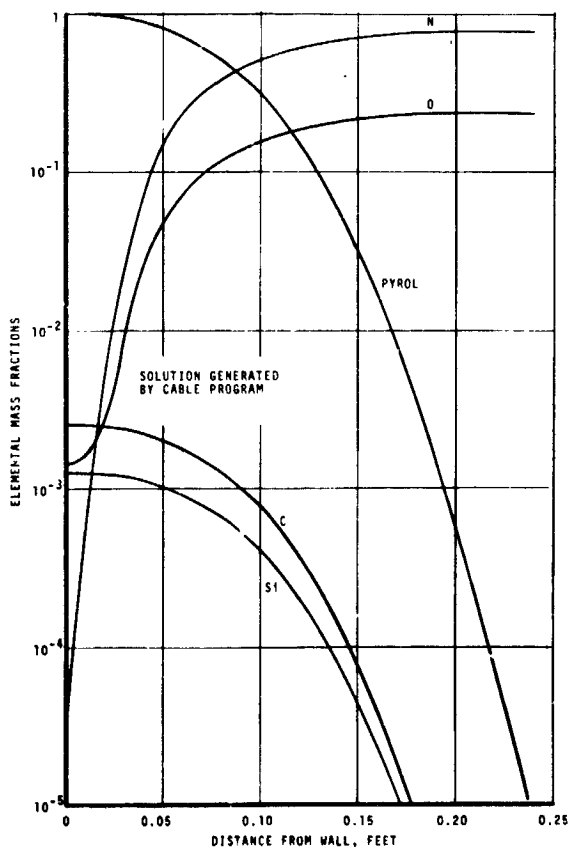


Figure 20. Elemental Mass Fractions Across Apollo Stagnation Point Boundary Layer During Typical Superorbital Reentry (Time = 30,020 sec)

TABLE III

CABLE RESULTS FOR TEMPERATURE DISTRIBUTIONS THROUGH THE CHARRING
ABLATOR AND BOUNDARY LAYER, PYROLYSIS GAS RATES, AND CHAR
RECESSION RATES: APOLLO STAGNATION POINT DURING
TYPICAL SUPERORBITAL REENTRY

Nodal Point	Distance from Surface, inch	Trajectory Times, sec					
		29,950	29,990	30,000	30,010	30,020	30,030
		Nodal Temperatures, °R					
<u>Boundary Layer</u>							
7 (edge)	See Concluding Portion of TABLE III on Next Page	12,230	15,040	16,500	17,870	18,700	18,860
6		12,070	14,970	16,500	17,870	18,660	18,840
5		10,120	13,120	14,420	15,240	15,590	15,220
4		7,416	9,169	7,417	7,434	8,545	11,440
3		6,796	7,562	2,673	2,760	4,105	8,699
2		4,002	4,088	1,870	2,167	3,498	6,823
1 (wall)		530	1,470	1,709	2,088	3,445	5,944
<u>Charring Ablator</u>							
1 (wall)	0	530	1,470	1,709	2,088	3,445	5,944
2	0.008		1,439	1,654	2,019	3,284	5,561
3	0.016		1,377	1,593	1,951	3,124	5,239
4	0.024		1,314	1,522	1,883	2,965	4,961
5	0.032		1,248	1,442	1,812	2,814	4,720
6	0.040		1,183	1,359	1,734	2,670	4,511
7	0.048		1,122	1,280	1,645	2,535	4,315
8	0.056		1,066	1,206	1,544	2,405	4,130
9	0.064		1,014	1,140	1,436	2,281	3,956
10	0.072		967	1,080	1,333	2,160	3,787
11	0.080		922	1,027	1,241	2,036	3,620
12	0.088		881	981	1,160	1,903	3,450
13	0.096		843	938	1,092	1,749	3,279
14	0.104		808	899	1,033	1,577	3,106
15	0.112		777	863	982	1,409	2,934
16	0.120		748	830	937	1,269	2,769
17	0.130		715	793	886	1,130	2,572
18	0.142		682	753	834	1,013	2,348
19	0.154		654	719	790	926	2,108
20	0.166		630	689	752	859	1,795
.
.
.
36	0.394		530	532	535	540	548
37	0.424		530	531	533	536	541
38 (backwall)	0.464	530	530	530	531	534	538

TABLE III (concluded)

	Trajectory Times, sec					
	29,950	29,990	30,000	30,010	30,020	30,030
Pyrolysis Gas Rate, lb/ft ² -sec x 10 ³	0	0.22	1.85	5.04	9.76	10.8
Char Recession Rate, lb/ft ² -sec x 10 ⁵	0	0	0.80	2.20	5.12	24.6
Boundary Layer Nodal Point	Distance from Surface, inch					
1	0	0	0	0	0	0
2	5.02	0.586	0.368	0.187	0.155	0.100
3	18.05	1.880	0.818	0.396	0.322	0.220
4	38.2	4.03	1.748	0.788	0.580	0.387
5	67.5	7.45	4.41	1.940	1.195	0.641
6	160.0	18.43	17.40	7.95	4.26	1.561
7	366	43.1	39.8	17.95	9.55	3.54

boundary layer edge is such as to result in a mass fraction of only 3.3×10^{-5} . The reader should keep in mind that CABLE requires the BLIMP subroutine to have 100 percent reliability while generating solutions such as these.

The above-described stagnation-point CABLE run, requiring 88 BLIMP solutions as well as time spent in CMA, consumed 29 minutes and 21 seconds on the Univac 1108 computer. This amounts to approximately 3 BLIMP solutions per minute at the stagnation point. (Experience has shown that 4 BLIMP solutions per minute are generated at downstream stations where faster convergence is achieved due to the better first guesses provided by the upstream station.) It is estimated that solution for an entire superorbital trajectory would require about one hour per streamwise station for the network of T_w , normalized char and pyrolysis gas rates, and times set up for the present case (see Appendix A). This could probably be reduced by a factor of two or so by setting up a somewhat coarser network.

SECTION 7

SUMMARY AND RECOMMENDATIONS

This report has summarized a substantial analytical effort which is reported in more detail in References 1 through 5 and in Parts II through IV of the present series of reports. The primary result of this effort has been the development of a number of computer codes applicable to charring ablation materials and chemically reacting boundary layers. For the most part, a modular approach has been utilized where the programs can be operated independently or used in conjunction with each other to obtain solutions with various degrees of coupling.

The basic programs which are described are the CMA program for predicting the transient in-depth response of charring ablation materials, the ACE program for predicting the chemical state of open or closed systems of arbitrary chemical composition, the RAD program for predicting nongrey radiation flux distributions for C-H-O-N systems, and the BLIMP program which represents the nonsimilar, laminar, multicomponent, chemically-reacting (equilibrium) boundary layer (using, in effect, the ACE program for calculating the chemical state at the boundary layer nodes and at the surface). A subroutine version of RAD has been incorporated into BLIMP to form the RABLE code for predicting radiation-coupled nonsimilar laminar boundary layers. The CMA code is used in conjunction with the ACE program (although mechanically decoupled) to provide an economical means for predicting coupled transient response of charring ablation materials with the boundary layer represented by laminar or turbulent transfer coefficients. The CABLE program calls the BLIMP and CMA programs as subroutines to provide fully coupled solutions for charring ablation materials and nonsimilar laminar boundary layers of arbitrary chemical composition. Finally, a turbulent extension of the BLIMP code has been initiated, resulting in the SAINT code which represents nonsimilar, constant property, turbulent boundary layers.

The physicochemical models considered in the CABLE program and its subroutines are summarized in Table I. As indicated therein, the code is applicable to arbitrary ablation materials, environmental gases, and two-dimensional flow situations. Coupled solutions have been attempted and successfully obtained only for the Apollo material; hence the CABLE program cannot be considered fully operational for all problems for which it is presumably applicable. However, no difficulties are anticipated in that the component codes, CMA and BLIMP, have been checked out for wide varieties of problems with

excellent success. The RAD code has been exercised extensively, whereas the RABLE code has been employed only seldom and thus must still be considered developmental.

The following recommendations are made with regard to improvement of these codes. In the first place, the ACE program, which was developed only as a byproduct of this study, should be cleaned up and documented. Secondly, the RABLE code should be exercised more extensively and for more severe problems and extended to encompass the entire shock layer. Thirdly, the non-similar turbulent boundary layer development should be continued with the ultimate product being a turbulent counterpart to BLIMP. In addition, BLIMP should be extended to three-dimensional flows and to treat general rate-controlled chemistry.

Probably an even more important recommendation is that the codes be employed now in their present status to current Apollo heating problems. Some of the types of calculations which can be performed with the codes are summarized in Section 6 of this report. They can be used, for example, to substantiate convective and radiative heating rates, to assess the validity of surface thermochemical ablation models and material thermal properties models, to predict radiation-convection coupling including absorption by ablation products, and to develop correlations to be used in more simplified analyses (e.g., blowing reduction parameters, heats of combustion, and correlations for radiation trapping and radiation coupling).

REFERENCES

1. Kendall, R. M., Bartlett, E. P., Rindal, R. A., and Moyer, C. B.: An Analysis of the Coupled Chemically Reacting Boundary Layer and Charring Ablator. Report No. 66-7, Part I, Aerotherm Corporation, Mountain View, California, March 14, 1967 (NASA CR-1060, June 1968).
2. Moyer, C. B. and Rindal, R. A.: Finite Difference Solution for the In-Depth Response of Charring Materials Considering Surface Chemical and Energy Balances. Report No. 66-7, Part II, Aerotherm Corporation, Mountain View, California, March 14, 1967 (NASA CR-1061, June 1968).
3. Bartlett, E. P. and Kendall, R. M.: Nonsimilar Solution of the Multi-component Laminar Boundary Layer by an Integral Matrix Method. Report No. 66-7, Part III, Aerotherm Corporation, Mountain View, California, March 14, 1967 (NASA CR-1062, June 1968). Also, Kendall, R. M. and Bartlett, E. P., AIAA J., 6, 1089, 1968.
4. Bartlett, E. P., Kendall R. M., and Rindal, R. A.: A Unified Approximation for Mixture Transport Properties for Multicomponent Boundary-Layer Applications. Report No. 66-7, Part IV, Aerotherm Corporation, Mountain View, California, March 14, 1967 (NASA CR-1063, June 1968).
5. Kendall, R. M.: A General Approach to the Thermochemical Solution of Mixed Equilibrium-Nonequilibrium, Homogeneous or Heterogeneous Systems. Report No. 66-7, Part V, Aerotherm Corporation, Mountain View, California, March 14, 1967 (NASA CR-1064, June 1968).
6. Bartlett, E. P. and Deblaye, C.: User's Manual Boundary Layer Integral Matrix Procedure (BLIMP). Report No. 68-42, Aerotherm Corporation, Mountain View, California, October 15, 1968.
7. Dorodnitsyn, A. A.: General Method of Integral Relations and its Application to Boundary Layer Theory. Advances in Aeronautical Sciences, Vol. 3, MacMillan, New York, 1960, pp. 207-219.
8. Pallone, A. J.: Nonsimilar Solutions of the Compressible-Laminar-Boundary Layer Equations with Applications to the Upstream-Transpiration Cooling Problem. J. Aerospace Sci., 28, 449, 1961.
9. Leigh, D. C. F.: The Laminar Boundary Layer Equation: A Method of Solution by Means of an Automatic Computer. Cambridge Phil. Soc. Proc., 51, 320, 1955.
10. Bartlett, E. P. and Grose, R. D.: The Multicomponent Laminar Boundary Layer over Graphite Sphere Cones: Solutions for Quasisteady Ablation and Application to Transient Reentry Trajectories. Report No. 68-35, Aerotherm Corporation, Mountain View, California, May 29, 1968 (to be issued as a Sandia Contractor's Report).
11. Aerotherm Corporation, Mountain View, California: User's Manual, Aerotherm Charring Material Ablation Program, Version 2, January 1966.
12. Aerotherm Corporation, Mountain View, California: User's Manual, Aerotherm Equilibrium Surface Thermochemistry Program, Version 2, June 1966.
13. Kendall, R. M., Rindal, R. A., and Bartlett, E. P.: A Multicomponent Boundary Layer Chemically Coupled to an Ablating Surface. AIAA J., 5, 1063, 1967.

REFERENCES (continued)

14. Van Driest, E. R.: Turbulent Boundary Layer in Compressible Fluids. J. Aero. Sci., 18, 145, 1951.
15. Kendall, R. M., Rubesin, M. W., Dahm, T. J., and Mendenhall, M. R.: Mass, Momentum, and Heat Transfer within a Turbulent Boundary Layer with Foreign Gas Mass Transfer at the Surface, Part I - Constant Fluid Properties. Report No. 111, Vidya Division of Itek Corporation, Palo Alto, California, February 1, 1964.
16. Clauser, F. H.: The Turbulent Boundary Layer. Advances in Applied Mechanics IV, 1956.
17. Kendall, R. M. and Anderson, L. W.: Nonsimilar Solution of the Incompressible Turbulent Boundary Layer. Presented at 1968 AFOSR-IFP-Stanford Conference on Turbulent Boundary Layer Prediction, Stanford University, August 1968 (to be published in proceedings).
18. Nicolet, W. E.: User's Manual - Radiation Transfer Code (RAD). Report No. 68-39, Aerotherm Corporation, Mountain View, California, October 15, 1968.
19. Wilson, K. H. and Nicolet, W. E.: JQSRT, 7, 891, 1967.
20. Biberman, L. M. and Norman, G. E.: Recombination Radiation and Bremsstrahlung of a Plasma, JQSRT, 3, 221, 1963.
21. Armstrong, B. H., Johnston, R. R., and Kelly, P. S.: Opacity of High Temperature Air. Report No. 8-04-64-2, Lockheed Missiles & Space Co., Sunnyvale, California, 1964 (also, AFWL-TR 65-17).
22. Griem, H. R.: Plasma Spectroscopy. McGraw-Hill Book Co., San Francisco, 1964.
23. Griem, H. R., Kolb, A. C., and Shen, R. V.: Stark Broadening of Hydrogen Lines in Plasma. NRL Report 5455, 1960.
24. Armstrong, B. H.: JQSRT, 4, 207, 1964.
25. Vorobyov, V. S. and Norman, G. E.: Energy Radiated in Spectral Lines by an Equilibrium Plasma, II. Optics & Spec., 14, 96, 1963.
26. Meyerott, R. E., Sokoloff, J., and Nicholls, R. A.: Absorption Coefficients of Air. Report No. LMSC-288052, Lockheed Missiles & Space Co., Sunnyvale, California, September 1959 (also Geophysics Res. Dir., GRO TR-60-277).
27. Biberman, L. M., Mnatsakanyan, A. Kh.: Optical Properties of Air in the Temperature Range from 4,000 to 10,000°K. Teplofizika Vysokikh Temperatur, 4, 148, 1966.
28. Allen, R. A.: Air Radiation Tables: Spectral Distribution Functions for Molecular Band Systems. Research Report 236, AVCO-Everett Research Laboratory, Everett, Massachusetts, April 1966.
29. Appleton, J. P. and Steinberg, M.: J. Chem. Phys., 46, 1521, 1967.
30. Arnold, J. O., Reis, V. H., and Woodward, H. T.: Studies of Shock-Layer Radiation of Bodies Entering Planetary Atmospheres. AIAA J., 2, 2019, 1965.

REFERENCES (concluded)

31. Weisner, J. D.: Hardening Technology Studies-II; Volume III, Aerothermodynamics; Part III, Radiative Properties. Report LMSC-B130391, Vol. III, Part III, Lockheed Missiles & Space Co., Sunnyvale, California, September 1966.
32. Evans, J. S. and Schexnayder, C. J., Jr.: An Investigation of the Effect of High Temperature on the Schumann-Runge Ultraviolet Absorption Continuum of Oxygen. NASA Technical Report R-92, 1961.
33. Churchill, D. R., Armstrong, B. H. and Mueller, K. G.: Absorption Coefficients of Heated Air: A Compilation to 24,000°. Report No. 4-77-65-1, Lockheed Missiles & Space Co., Sunnyvale, California, 1965.
34. Chandrasekhar, S. and Elbert, D. D. : On the Continuous Absorption Coefficient of the Negative Hydrogen Ion. V. Astrophys. J., 128 114, 1958.
35. Seman, M. and Branscomb, L. M.: Phys. Rev., 125, 1602, 1962.
36. Morris, J. C., Bach, G. R., Krey, R. U., Liebermann, R. W. and Yos, J.M.: AIAA J., 4, 1223, 1966.
37. Hunt, B. L. and Sibulkin, M.: Radiation Transfer in a Gas of Uniform Properties in Local Thermodynamic Equilibrium, Parts I, II, and III. Report No. NONR-562(35)/18, Brown University, Providence, Rhode Island, December 1966.
38. Schaefer, J. W., Flood, D. T., Reese, J. J., Jr., and Clark, K. J.: Experimental and Analytical Evaluation of the Apollo Thermal Protection System Under Simulated Reentry Conditions. Report No. 67-16, Parts I and II, Aerotherm Corporation, Mountain View, California, July 15, 1967.

APPENDIX A
AN ILLUSTRATION OF THE CABLE COUPLING PROCEDURE
FOR A TYPICAL APOLLO SUPERORBITAL
REENTRY TRAJECTORY

APPENDIX A

AN ILLUSTRATION OF THE CABLE COUPLING PROCEDURE FOR A TYPICAL APOLLO SUPERORBITAL REENTRY TRAJECTORY

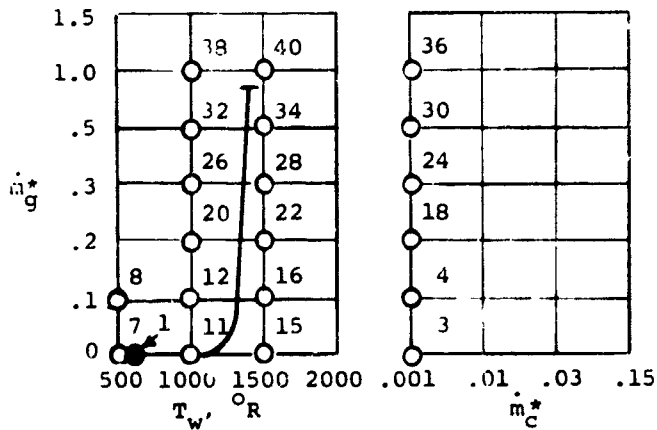
The results of a coupled transient solution at the stagnation point of the Apollo heat shield during the first 80 seconds of a recent Apollo super-orbital flight were presented in Section 6.8 of this report. In this appendix, the sequence of BLIMP solutions which were required during the course of that calculation are discussed in some detail in order to illustrate the coupling procedure employed in the CABLE program. Solutions are also shown for a second streamwise station which illustrate how the solution proceeds around the body.

In this problem, the time-table entries were selected to be 29,950, 29,990, 30,000, 30,010, 30,020 and 30,030 seconds. The \dot{m}_g^* entries were taken to be 0, 0.1, 0.2, 0.3, 0.5, 1.0 and 1.5 with T_w entries of 500, 1,000, 1,500, 2,000, and 2,500°R and \dot{m}_c^* entries of 0.001, 0.010, 0.03 and 0.15. As discussed in Section 2.5, boundary-layer solutions are performed at combinations of these independent parameters as they are required; they are numbered in Figure A-1 in the sequence in which they were performed in the present problem.

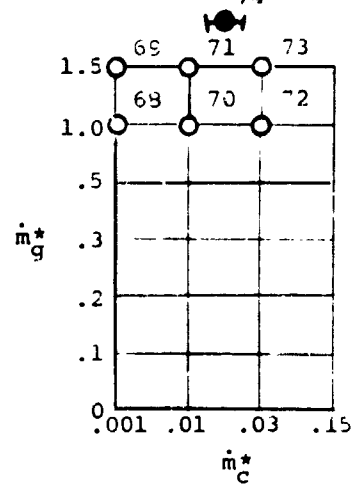
The first step in the coupled solution was to initialize the charring ablation solution at the assumed initial temperature of 530°R. This was followed by a boundary-layer solution at this initial nonablating condition ($\theta_1 = 29,950$ sec, $T_w = 530^\circ\text{R}$, $\dot{m}_g^* = 0$). This is identified as Solution 1 in Figure A-1. The next step was to find the wall temperatures at which ablation would start for the initial times of 29,950 seconds and the second entry in the time table, 29,990 seconds, each for the first two entries in the \dot{m}_g^* table, namely 0 and 0.1 (Solutions 2 through 5). This was accomplished by computing the surface temperatures required to maintain surface equilibrium for these boundary-layer edge conditions (i.e., times), these normalized pyrolysis gas flow rates, and a very small normalized surface recession rate (\dot{m}_c^* of 0.001 was used in these boundary-layer calculations). The resulting "ablation temperatures" were at the silica fail temperature of 1,620°R, higher than the first two entries in the T_w table of 500 and 1,000°R. Therefore, T_w was the appropriate independent parameter (rather than \dot{m}_g^*) during this portion of the trajectory. Boundary-layer solutions were then obtained at the eight corners of the θ_1 , \dot{m}_g^* , T_w cube (Solutions 6 through 13). At this point the transient charring-ablation solution was able to commence, interpolating between the bracketing values of θ_1 , \dot{m}_g^* and T_w .

A-2

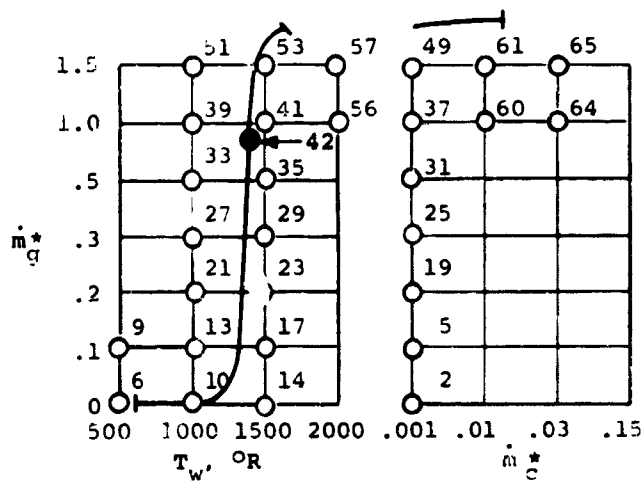
$\theta_1 = 29,950 \text{ SEC}$



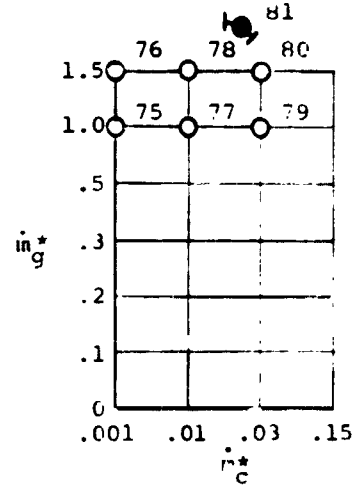
$\theta_4 = 30,010 \text{ SEC}$



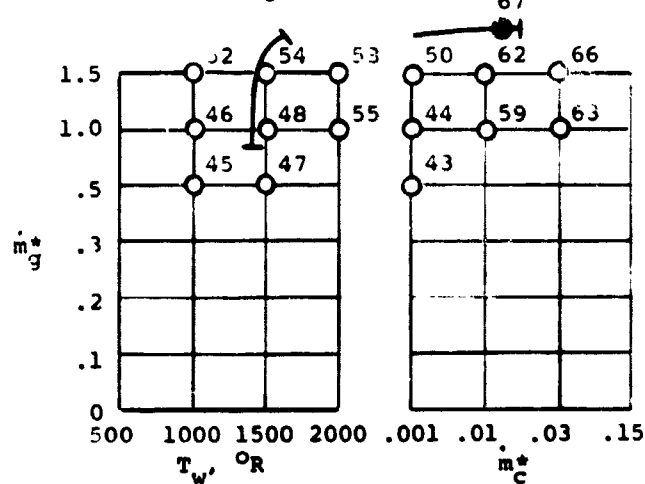
$\theta_2 = 29,990 \text{ SEC}$



$\theta_5 = 30,020 \text{ SEC}$



$\theta_3 = 30,000 \text{ SEC}$



$\theta_6 = 30,030 \text{ SEC}$

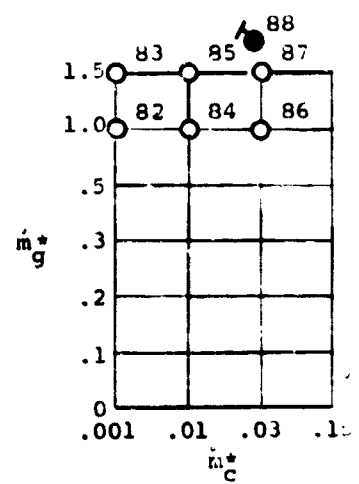


Figure A-1. Sequence of BLIMP Solutions Required in CABLE Solution for Typical Superorbital Apollo Reentry

The transient charring-ablation solution then proceeded toward $\theta_2 = 29,990$ seconds, the time steps being determined by various controls built into the implicit finite-difference procedure. However, before reaching this time, a T_w of $1,000^\circ\text{R}$ and later a \dot{m}_g^* of 0.1 were exceeded. Therefore, BLIMP solutions were generated for the two current times and current \dot{m}_g^* for a T_w of $1,500^\circ\text{R}$ (Solutions 14 through 17); ablation temperature (surface equilibrium) BLIMP solutions were generated for the current times for the next \dot{m}_g^* entry of 0.2 (Solutions 18 and 19); solutions were generated for the current times and T_w (now $1,000$ and $1,500^\circ\text{R}$) at \dot{m}_g^* of 0.2 (Solutions 20 through 23); and ablation temperatures were generated and matrix points filled in for \dot{m}_g^* of 0.3 (Solutions 24 through 29), for \dot{m}_g^* of 0.5 (Solutions 30 through 35), and for \dot{m}_g^* of 1.0 (Solutions 36 through 41). Within the currently bracketed conditions of T_w of $1,000$ and $1,500^\circ\text{R}$ and \dot{m}_g^* of 0.5 and 1.0, the CMA program finally advanced to 29,990 seconds. A charring ablation solution was performed precisely at this time, and this was followed by a boundary layer solution at the same time, wall temperature, \dot{m}_g^* and \dot{m}_c^* (Solution 42). The next order of business was to obtain the ablation temperatures (Solutions 43 and 44) at the next entry in the time table ($\theta_3 = 30,000$ seconds) for the two current \dot{m}_g^* of 0.5 and 1.0, and to obtain boundary-layer solutions at this new time for the two current T_w and \dot{m}_g^* (Solutions 45 through 48).

The transient charring-ablation solution was then able to recommence and continue until a \dot{m}_g^* of 1.0 was attained. It was then necessary to perform ablation temperature calculations at the next \dot{m}_g^* entry of 1.5 (Solutions 49 and 50) and boundary layer solutions for this \dot{m}_g^* and the current bracketing values of time and T_w (Solutions 51 through 54). The charring-ablation solution then recommenced and continued until a T_w of $1,500^\circ\text{R}$ was attained. Boundary layer solutions were then generated for the next T_w entry of $2,000^\circ\text{R}$ for the current times (29,990 and 30,000 sec) and \dot{m}_g^* (1.0 and 1.5) under consideration (Solutions 55 through 58). Shortly thereafter a \dot{m}_g^* of 1.5 was exceeded. However, since 1.5 was the largest entry in the input matrix, the CMA solution proceeded by extrapolating from the current entries of \dot{m}_g^* of 1.0 and 1.5, T_w of $1,500$ and $2,000^\circ\text{R}$, and times of 29,990 and 30,000 seconds. (A maximum \dot{m}_c^* of 2.803 was encountered later in the trajectory, at 30,015 seconds. This extrapolation caused no computational difficulties and only slightly reduced the accuracy of the final solution since B'_g has only a minor effect for the assumed surface thermochemistry model.)

When the CMA solution reached the ablation temperature of $1,620^\circ\text{R}$, it was necessary to change from T_w to \dot{m}_c^* as one of the three independent variables (retaining \dot{m}_g^* and θ_1). The ablation temperature calculations for \dot{m}_c^* of

0.001 serve as one side of the cube; hence, it was necessary only to generate BLIMP solutions at the next \dot{m}_c^* entry of 0.01 for the two current times and \dot{m}_g^* (Solutions 59 through 62). The CMA solution then recommenced but only briefly since \dot{m}_c^* of 0.01 was soon attained. Solutions were then generated for the next \dot{m}_c^* entry of 0.03 for the current times and \dot{m}_g^* (Solutions 63 through 66). The charring ablation solution then recommenced and continued until the tabular entry time of 30,000 seconds, at which point a boundary layer solution was obtained (Solution 67). In order to proceed further with the charring ablation solution, it was necessary to generate boundary layer solutions to obtain ablation temperatures* (Solutions 68 and 69) and to fill in the matrix for the current \dot{m}_g^* and \dot{m}_c^* (Solutions 70 through 73) for the next time entry, 30,010 seconds. The CMA solution was reinitiated and continued until 30,010 seconds at which point a boundary layer solution was again generated (Solution 74). This process was repeated for the last two time entries, 30,020 and 30,030 seconds, resulting in CMA and BLIMP solutions at these times (Solutions 81 and 88). With 30,030 seconds being the last entry in the time table, the solution moved on to the second streamwise station.

The identical process was repeated at the second station during the initial setup period. The first 41 solutions at this station (Solutions 89 through 129) corresponded to the same matrix points as Solutions 1 through 41 which were performed at the stagnation point. The sequence differed from here on because the surface temperature exceeded 1,500°R and the \dot{m}_g^* exceeded 1.0 before the 29,990 second time entry was attained. This particular solution was terminated at 29,990 seconds (Solution 140).

* It is necessary to calculate ablation temperatures when ablation is occurring, as well as when ablation is not occurring, in order to know when to terminate ablation and exchange \dot{m}_c^* for T_w as an independent variable.